Sensitivity of Tropical Tropospheric Composition to Lightning NO_x Production

Christina E. Liaskos

Dale J. Allen and Kenneth E. Pickering

In Partial Fulfillment of the Requirements for the Degree of Master of Science

Department of Atmospheric and Oceanic Science

University of Maryland, College Park

Abstract

The sensitivity of tropical tropospheric composition to the source strength of nitrogen oxides (NO_x) produced by lightning (LNO_x) is analyzed for the September-to-November 2007 time period using NASA's GEOS-5 global Chemistry-Climate Model (CCM); satellite retrievals from OMI, TES and OMI/MLS; and in situ measurements from SHADOZ ozonesondes. Global LNO_x production rates of 0 to 10 Tg N a^{-1} and the subsequent responses of NO_x, ozone (O_3), hydroxyl radical (OH), nitric acid (HNO_3), peroxyacetyl nitrate (PAN) and NO_y (NO_x + HNO_3 + PAN) are investigated. The radiative implications associated with LNO_x-induced changes in tropospheric O_3 are assessed. Increasing the LNO_x source strength by a factor of 4 (from 2.5 to 10 Tg N a^{-1}) leads to tropical upper-tropospheric enhancements of more than 100 % in NO_x, OH, HNO_3 and PAN. This increase in LNO_x also leads to O_3 enhancements of up to 60 %, which subsequently yields a factor-of-three increase in the mean net radiative flux at the tropopause. Comparisons with observations indicate that the 5.0 Tg N a^{-1} source is most realistic, since the 2.5 Tg N a^{-1} source underestimates tropospheric columns of NO_2 and the 10 Tg N a^{-1} source overestimates tropospheric columns of O_3. Biases in modeled LNO_x, due to regional biases in modeled flashes and/or regional differences in the NO production per flash, add uncertainty to this analysis. Further research into understanding the regional dependence of LNO_x production should help resolve the discrepancies that currently exist between the model and observations.

Contents

1. Introduction

Nitrogen oxides ($NO_x \equiv NO + NO_2$) play an important role in tropospheric chemistry. They are catalytic precursors of ozone (O_3) and they strongly influence the oxidative capacity of the atmosphere via production of the hydroxyl radical (OH) [*Jourdain and Hauglustaine*, 2001; *Zhang et al.*, 2003; *Kunhikrishnan and Lawrence*, 2004; *Labrador et al.*, 2005]. NO_x sources are both natural and anthropogenic, originating from fossil fuel combustion, biomass burning, soil release, ammonia oxidation and lightning, as well as from stratospheric exchanges and aircraft emissions [*Stockwell et al.*, 1999; *Zhang et al.*, 2003]. In the tropical upper troposphere (UT), lightning dominates NO_x production and, as a result, has a profound impact on tropical tropospheric photochemistry [*Jourdain and Hauglustaine*, 2001; *Bond et al.*, 2002].

The distribution of NO_x in the atmosphere is affected by emissions, nitrogen oxide reservoir species, photochemistry, dry depositional losses and meteorological conditions, but is not well understood. The most uncertain component of the NO_x budget is lightning [*Allen et al.*, 2012]. Considerable uncertainty remains in both the magnitude and the distribution of lightning-produced NO_x (LNO_x), with most recent global estimates varying between 2 and 8 Tg N a^{-1} [*Schumann and Huntrieser*, 2007; *Wang et al.*, 2013]. Reasons for the large uncertainty in LNO_x production are related to (a) poorly understood aspects of the lightning phenomenon and associated LNO_x production process, (b) scalability of local measurements to the global atmosphere, and (c) uncertainty in global flash rates and lightning distribution [*Beirle et al.*, 2004; *Labrador et al.*, 2005].

Two types of information are needed to estimate the global LNO_x source strength: the global flash rate and the mean production of NO per flash. The global number of flashes has been fairly well established by climatologies constructed from satellite sensors, such as the

Optical Transient Detector (OTD, 1995-2000) [*Boccippio et al.*, 2000; *Christian et al.*, 2003] and the Lightning Imaging Sensor (LIS, 1997-present) [*Christian et al.*, 2003; *Boccippio et al.*, 2002; *Mach et al.*, 2007; *Cecil et al.*, 2014]. Recent global flash rate estimates, based on observations from OTD and LIS, average 46 flashes per second, with a range of 35 to 60 flashes per second [*Cecil et al.*, 2014]. Therefore, the factor-of-four uncertainty currently associated with the global LNO_x source strength stems primarily from the uncertainty in the global mean NO_x production per flash. Several methods have been used to estimate this quantity: theoretical estimates [*Price et al.*, 1997; *Koshak et al.*, 2014], laboratory experiments [*Wang et al.*, 1998], cloud-resolving model simulations constrained by lightning flash observations and anvil NO_x measurements [*DeCaria et al.*, 2005; *Ott et al.*, 2007, 2010; *Cummings et al.*, 2013], analysis of aircraft data [*Huntrieser et al.*, 2008, 2009, 2011], and analyses of satellite observations [*Beirle et al.*, 2004, 2006, 2010; *Bucsela et al.*, 2010]. NO_x production estimates from these studies vary from 30 to 1100 moles per flash, though most estimates fall between 100 and 500 moles per flash. Furthermore, *Huntrieser et al.* [2008] have found that flashes in tropical thunderstorms tend to produce less NO_x than flashes in subtropical and extratropical storms. They have hypothesized that greater vertical wind shear at higher latitudes leads to greater flash lengths and, thus, greater LNO_x production per flash. The uncertainty in the global mean production of NO_x may be reduced with the use of satellite-based observations of trace gases related to LNO_x chemistry [*Martin et al.*, 2007], such as nitrogen dioxide (NO_2) and O_3. In situ measurements of nitric acid (HNO_3) deposition may also contribute as a top-down constraint for estimating the NO_x produced by lightning.

Lightning directly deposits NO_x primarily into the middle and upper troposphere. After convective transport, the greatest fraction resides between 6 and 10 km [*Pickering et al.*, 1998;

Ott et al., 2010]. In contrast, surface NO_x emissions reside primarily within the planetary boundary layer (PBL) [*Zhang et al.*, 2003]. Since NO_x lifetime varies considerably with altitude, from a few hours near the surface to a few days in the UT, NO_x emitted directly into the middle and upper troposphere more effectively perturbs the concentrations of NO_x and other chemically-relevant trace gas species [*Jourdain and Hauglustaine*, 2001; *Zhang et al.*, 2003; *Labrador et al.*, 2005, *Martin et al.*, 2007]. Thus, although the lightning component of the total NO_x budget is relatively small, its contribution to upper-tropospheric NO_x chemistry is substantial.

In the tropics and subtropics, LNO_x is estimated to contribute more than 70 % of the NO_x in the UT [*Schumann and Huntrieser*, 2007]. Increases in NO_x due to lightning generally lead to enhancements in O_3 and OH [*Labrador et al.*, 2005], particularly in regions of low NO_x concentrations [*Schumann and Huntrieser*, 2007]. When NO_2 reacts with OH, it leads to the formation of HNO_3; *Martin et al.* [2007] have found that LNO_x oxidation explains nearly 80 % of the annual mean tropical (30°N to 30°S) HNO_3 at 200 to 350 hPa. In the stratosphere and UT, HNO_3 is recycled back to NO_x, via photolysis and reaction with OH, on a time scale of a few weeks [*Jacob*, 1999]. In the lower troposphere (LT), however, HNO_3 is readily scavenged by precipitation, due to its high solubility in water, on the order of a few days [*Jacob*, 1999]. As a result, HNO_3 in the UT serves as an important reservoir for odd nitrogen [*Zhang et al.*, 2003, *Kunhikrishnan and Lawrence*, 2004], whereas near the surface it acts primarily as a NO_x sink. A portion of lightning-produced NO_x gets converted to peroxyacetyl nitrate (PAN), which has a relatively long lifetime in the cold UT [*Schumann and Huntrieser*, 2007] and thus acts as an effective NO_x reservoir. The lifetime of PAN is highly temperature dependent, ranging from one hour at 295 K to several months at 250 K [*Jacob*, 1999]; thermal decomposition of PAN resulting from adiabatic subsidence is the principal source of NO_x in the remote troposphere.

Both HNO_3 and PAN have relatively long upper-tropospheric lifetimes and can therefore be transported over long distances, where they then break down and release NO_x far from the initial source [*Staudt et al.*, 2003].

Lightning plays an important role with respect to climate, as LNO_x production occurs primarily in the tropical UT, where O_3 acts most efficiently as a greenhouse gas [*Lacis et al.*, 1990; *Stockwell et al.*, 1999; *Zhang et al.*, 2003; *Kunhikrishnan and Lawrence*, 2004; *Dahlmann et al.*, 2011] and where high UV radiation, low background NO_x and long O_3 lifetime lead to very high O_3 production efficiency (approximately 100 molecules of O_3 per molecule of NO_x) [*Dahlmann et al.*, 2011]. Conversely, lightning also influences the oxidative capacity and radiative forcing of the atmosphere through its effect on OH: increased LNO_x promotes increased OH formation, which in turn oxidizes methane (a greenhouse gas) and leads to subsequent short-term radiative cooling [*Kunhikrishnan and Lawrence*, 2004].

Several modeling studies have addressed how the strength of the LNO_x source impacts tropospheric composition. *Stockwell et al.* [1999] noted better agreement with observations after including LNO_x production in their model, equating to an approximate doubling of NO_x in the equatorial UT. They also observed increases of greater than 40 % in O_3, of greater than 100 % in HNO_3 and of 50 % in OH near 300 hPa. Similarly, *Labrador et al.* [2005] observed lightning-induced enhancements in NO_x throughout the middle and upper troposphere (between 200 and 800 hPa) between 40°N and 40°S, peaking near 300 hPa over the equator. The largest enhancements in NO_x, O_3, OH, HNO_3 and PAN were observed at 300 to 500 hPa. According to *Chandra et al.* [2004], the lightning contribution to tropospheric column ozone (TCO) was 20 to 30 % in the tropics and 10 to 15 % in the midlatitudes over the Atlantic and Pacific oceans. Budget analyses performed by *Zhang et al.* [2003] showed that lightning contributes more than

50 % of the upper-tropospheric NO_x over the United States from April to November, impacting the upper-tropospheric O_3 budget by as much as 30 %. Combined measurement and modeling studies performed by *Cooper et al.* [2006, 2007] indicated that LNO_x production led to upper-tropospheric O_3 enhancements of 25 to 30 ppbv in the southern U.S. during August 2006 and of 11 to 13 ppbv over eastern North America during July through August 2004. At many locations, O_3 increases with altitude due to: (a) upper-tropospheric LNO_x production, (b) reduced chemical loss caused by decreased water vapor (and hence HO_x) [*Jacob*, 1999; *Martin et al.*, 2000] and (c) isentropic cross-tropopause transport of O_3 from the stratosphere [*Allen et al.*, 2003; *Jing et al.*, 2005].

In this study, we use a global chemistry-climate model and a suite of observational data sets to investigate the sensitivity of tropical tropospheric composition to the LNO_x source strength. In particular, we examine the significance of LNO_x with respect to the concentration and distribution of NO_x, O_3, OH, HNO_3, PAN and NO_y (herein defined as $NO_x + HNO_3 + PAN$) within the tropical troposphere. We focus on these particular species because they play important roles in tropospheric NO_x chemistry, air quality and climate. We then consider the climate implications associated with changes in radiative forcing attributable to LNO_x-induced changes in tropospheric O_3.

2. Methodology

2.1 GEOS-5 Chemistry-Climate Model

The National Aeronautics and Space Administration (NASA) Goddard Space Flight Center (GSFC) Chemistry-Climate Model (CCM) used in this study includes version 5 of the NASA Goddard Earth Observing System General Circulation Model (GEOS-5 GCM) and the

NASA Global Model Initiative (GMI) Chemical Transport Model (CTM). It is run using a horizontal resolution of 2.0° latitude × 2.5° longitude and a vertical resolution of 72 layers with a model top of 0.01 hPa. A combined troposphere/stratosphere (i.e., the 'Combo') chemical mechanism is used, which contains 117 species, 322 chemical reactions and 81 photolysis reactions [*Duncan et al.*, 2007]. Biogenic emissions of isoprene and monoterpenes are calculated on-line, and time-appropriate biomass burning emissions are provided using version 3 of the Global Fire Emissions Database (GFED3) [*van der Werf et al.*, 2010].

The CCM is run in "replay mode", utilizing reanalysis data from the Modern-Era Retrospective Analysis for Research and Applications (MERRA) [*Rienecker et al.*, 2011] to constrain model dynamics. This study may be the first to use the CCM in this mode, with a major benefit being the facility to focus on a particular time period without allowing dynamical uncertainties and nonlinearities to develop in the model. By constraining the CCM to observations, we are able to perform sensitivity studies using a small number of simulations with less run-to-run uncertainty. More information on the CCM and "replay mode" can be found in Appendix I.

2.2 Parameterization of flash rates in the GEOS-5 CCM

The CCM in this study employs a simple flash rate parameterization, which incorporates two variables correlated to flash rate: normalized integrated cold-core (temperature less than 263 K) convective mass flux (X_4) and normalized cubed surface temperature perturbation from 273 K (X_5), and is expressed as follows:

$$Y = a\,[X_4 + X_5]. \qquad (1)$$

The constant *a* is set to 0.003 at marine locations with convective precipitation and to 0.053 at continental locations with convective precipitation, which leads to a reasonable continental/marine partitioning of flashes and a global annual mean flash rate of 46 flashes per second for the five-year training period, which matches the OTD/LIS version 2.2 climatology [*Cecil et al.*, 2014]. Global LNO_x sources of 2.5, 5.0 and 10 Tg N a^{-1} are obtained by using production rates of 125, 250 and 500 moles per flash. See Appendix II for more information regarding the flash rate parameterization employed in the CCM for this study.

2.3 Sensitivity Studies

The NASA GEOS-5 CCM with this LNO_x algorithm and a 5.0 Tg N a^{-1} source has been used to simulate the June 2006-to-February 2008 time period. For this study, we focus on September through November (SON) 2007, for which we performed four sensitivity experiments (all initialized in July 2007 from the base "stdLNOx" run and integrated through December 2007). The first sensitivity simulation (henceforth referred to as the default run, or dfLNOx) uses monthly-varying flash rates and a 5.0 Tg N a^{-1} source. In this simulation, LNO_x is continuously bled into the model, with the production rate at each grid box chosen to be proportional to the OTD/LIS climatological flash rate at that location. This approach ensures that the location of the LNO_x is consistent with the climatological distribution of flashes. However, the location of model lightning is not necessarily consistent with the location of model convection. The vertical partitioning of the LNO_x in the dfLNOx simulation is chosen such that, when averaged over a one-month period, it matches the mean vertical distribution for that month from a multi-year simulation with the GMI model [*Allen et al.*, 2010].

The base simulation and the remaining three sensitivity simulations parameterize model flash rates with respect to modeled convective parameters (see Section 2.2 and Appendix II). The main difference between these simulations and the dfLNOx simulation is the episodic 'pulse' of LNO_x into regions of convection, rather than the steady bleeding of LNO_x into the same location over time. The use of pulsed emissions ensures that modeled LNO_x is consistent with modeled meteorology and precursor distribution of chemical species. However, the location of model LNO_x is not necessarily consistent with the location of observed flashes.

The LNO_x production rates for the three sensitivity runs are set to 0 (noLNOx), 125 (.5xLNOx) and 500 (2xLNOx) moles per flash. The .5xLNOx and 2xLNOx simulations represent plausible lower and upper bounds of the accepted range for LNO_x source strength, while the noLNOx run serves to isolate the effects of lightning from other NO_x sources.

3. Significance of LNO_x for tropical tropospheric composition

3.1 Effect of LNO_x on the horizontal distribution of trace gas species

Lightning-induced changes in NO_x concentrations are most evident in the UT, where LNO_x production is large and where the contributions from surface sources are small. Figure 1 shows the mean 200- to 400-hPa NO_x, averaged over SON 2007, for the (a) noLNOx, (b) .5xLNOx, (c) stdLNOx and (d) 2xLNOx simulations. In the tropics (henceforth defined as 22°N to 22°S), removing, halving and doubling the stdLNOx production rate of 250 moles per flash lead to changes in upper-tropospheric NO_x of -56 % (-35 ppt), -29 % (-18 ppt) and +59 % (+37 ppt), respectively.

Lightning occurs preferentially over land because many marine updrafts are too weak to form substantial charge separation in the cloud, and because mixed-phase microphysical

processes are more common at continental locations. In the tropics, 35 % of the LNO_x modeled for the SON 2007 time period originates over Africa (30°W to 60°E), while 34 % originates over South/Central America (120°W to 40°W) and 27 % originates over Southeast Asia, southern India and northern Australia (60°E to 170°E) (not shown). Similar calculations performed by *Martin et al.* [2000], who analyzed global lightning NO_x emissions estimates from *Price et al.* [1997], showed the percentage of LNO_x produced within 15°N and 15°S to be 28 % over Africa, 34 % over South America and 38 % over Southeast Asia and Oceania.

Since model dynamics and non-lightning source emissions are kept constant for all model simulations, we are able to isolate changes in tropospheric composition due to lightning alone by examining the differences between each sensitivity simulation. In this regard, we compare the noLNOx, .5xLNOx and 2xLNOx simulations, relative to the stdLNOx simulation, to investigate lightning-induced changes in upper-tropospheric NO_x, O_3 and OH (Figure 2), and NO_y, HNO_3 and PAN (Figure 3). The stdLNOx run is chosen as the baseline for these comparisons because it falls in the middle of the currently-accepted range for LNO_x production.

When all LNO_x is removed (Xi = 0), greater than 20 % reductions in NO_x, O_3, OH, NO_y, HNO_3 and PAN occur throughout the tropical UT, with reductions of more than 80 % in NO_x over equatorial South America, western Africa and Indonesia. The effect of removing LNO_x on different trace gases varies greatly both in magnitude and in spatial distribution. Regions with greater than 80 % reductions in NO_x also show localized decreases of up to 60 % in O_3, 80 % in OH, NO_y and HNO_3, and more than 80 % in PAN.

When LNO_x production is reduced to 125 moles per flash (Xi = .5xLNOx), maximum NO_x reductions of 40 to 60 % are observed over equatorial South America, western Africa and Indonesia, with greater than 20 % NO_x reductions occurring throughout most of the tropics.

This correlates with relatively uniform reductions of 10 to 20 % in O_3 and of 20 to 40 % in HNO_3 and NO_y. Reductions in OH and PAN are more spatially varied, with decreases of 10 to 20 % broadly covering the tropics and decreases of 20 to 60 % surrounding the high-NO_x regions of South America, Africa and Southeast Asia.

Doubling LNO_x to 500 moles per flash (Xi = 2xLNOx) leads to NO_x enhancements of greater than 20 % throughout the tropics, with maximum increases of approximately 100 % located over regions of high lightning activity, such as northern South America, equatorial western Africa and maritime Southeast Asia. The subsequent O_3 enhancements over the same regions amount to less than half of that, about 20 to 40 %. OH shows high sensitivity to doubled LNO_x, especially over the equatorial continents, where the changes in OH (up to more than 100 %) are highly correlated in space and magnitude with the changes in NO_x. HNO_3 shows enhancements of more than 40 % throughout the tropics, with broad increases of 60 to 80 % over much of the tropical Atlantic and southern Africa and increases of up to 100 % over Micronesia. Increases in PAN of 20 to 40 % cover the majority of the globe south of 15°N. Localized PAN enhancements are also observed over much of South America (40 to 100 %) and eastern maritime Southeast Asia (40 to 80 %).

The horizontal distribution of LNO_x-related changes in tropospheric composition varies greatly depending on the lifetime of the trace gas considered. Species with relatively long upper-tropospheric lifetimes (e.g., O_3, approximately 1 month) tend to show broad, moderate changes, whereas relatively short-lived species (e.g., OH, roughly 1 s) tend to show more intense and localized responses. This study helps to validate this a priori assumption regarding the characteristic response of a trace gas to the perturbation source as a function of its lifetime.

3.2 Effect of LNO_x on the vertical distribution of trace gas species

Section 3.1 demonstrates that changes in upper-tropospheric composition coincide with changes in LNO_x production, and that the horizontal distribution of these changes is co-located with active lightning regions. This section aims to supplement the previous section by investigating the influence of LNO_x production on the *vertical* distribution of tropical tropospheric composition.

Increasing LNO_x production by a factor of 4 (from 2.5 to 10 Tg N a^{-1}) leads to NO_x enhancements throughout the middle and upper troposphere, peaking at approximately 150 % over the equator within the 200- to 450-hPa pressure layer (Figure 4). In contrast, NO_x *reductions* of up to 10 % are evident throughout the tropical and extratropical PBL, as well as in the northern lower to middle troposphere. This is consistent with results from *Stockwell et al.* [1999] and *Labrador et al.* [2005], and results from increased conversion of NO_2 to HNO_3 via reaction with OH, and increased conversion of NO_2 to NO_3 (and ultimately N_2O_5) via reaction with O_3. Both OH and O_3 concentrations increase when LNO_x is increased; NO_x decreases because the subsequent loss of HNO_3 by hydrolysis on aerosols [*Dentener and Crutzen,* 1993] locally exceeds the increases in NO_x due to LNO_x production.

O_3 changes are less profound in magnitude, but have a greater vertical extent when compared to changes in NO_x. Maximum enhancements of 40 to 60 % occur in the 200- to 750-hPa layer between 15°N and 15°S, with increases of 10 to 40 % extending toward the surface between 30°N and 30°S. LNO_x is produced in the tropical UT, where the lifetime of O_3 is relatively long. As a result, O_3 produced from lightning is able to survive long-distance transport outward and downward from the LNO_x source region, resulting in the ovular signature seen in Figure 4b.

The sensitivity of OH more closely resembles NO_x with respect to the shape and the magnitude of its response, primarily due to its very short lifetime. Peak OH enhancements of 80 to 150 % occur in the 200- to 400-hPa layer, where increases in NO_x are also maximized. Although changes of up to 40 % extend downward into the tropical PBL, the most significant changes occur in the middle to upper troposphere.

At pressures lower than 700 hPa, the impact of increased LNO_x leads to widespread increases in HNO_3 extending well into the northern and southern extratropics. At pressures greater than 700 hPa, HNO_3 changes are localized, with the largest enhancements constrained between 10°N and 10°S. The magnitude of the HNO_3 response to LNO_x is consistent with NO_x, but the shape and vertical distribution are not. Peak HNO_3 change is centered around 500 hPa, which is closer to the surface when compared to NO_x.

The sensitivity of PAN to changing LNO_x takes on a very long and narrow shape, with increases of 80 to 150 % centered over the equator and stretching from 150 to 900 hPa. PAN enhancements of 10 to 20 % extend to the surface, but are confined to the equatorial and Southern-Hemisphere tropics (approximately 15°S).

Figure 5 shows mean tropical atmospheric profiles for NO_x, O_3, OH, NO_y, HNO_3 and PAN, averaged over SON 2007. Increasing the LNO_x source strength leads to distortions in the shape of the profiles for NO_x, OH, NO_y, HNO_3 and PAN, most noticeably with regard to the 2xLNOx simulation. Extensive profile "bulging" is evident in the 2xLNOx profiles of NO_x (200 to 500 hPa), OH (200 to 700 hPa), NO_y (150 to 600 hPa), HNO_3 (150 to 800 hPa) and PAN (100 to 800 hPa). In the case of O_3, increased LNO_x leads to a rightward shift in the profile, however, the shape of the profile itself is minimally affected.

3.3 Correlation of tropical upper-tropospheric chemistry with lightning flash rate

The impact of LNO_x source strength on tropical upper-tropospheric composition, and the correlation of that impact with lightning flash rate, vary significantly by region and by trace gas species considered. Figure 6 displays the changes in upper-tropospheric NO_x (a-c), O_3 (d-f), HO_x ($HO_x \equiv HO_2 + OH$) (g-i), NO_2/NO (j-l) and HO_2/OH (m-o) between the .5xLNOx and 2xLNOx simulations versus flash rate for South America (red), Africa (purple) and Southeast Asia (blue). As expected, increasing NO production per flash leads to enhancements in upper-tropospheric NO_x, which are highly correlated with local flash rate. However, the sensitivity of upper-tropospheric NO_x to flash rate exhibits regional variations, with flashes over Africa producing greater change in NO_x than flashes over South America or Southeast Asia. Upper-tropospheric O_3 increases by 20 to 30 ppb over South America and Africa and by 10 to 15 ppb over Southeast Asia when LNO_x production is increased by a factor of 4; however, local changes in O_3 are not correlated with local changes in flash rate. This result shows that changes in upper-tropospheric O_3, which has a relatively long lifetime, are more closely related to advection of O_3 and O_3 precursors than to local LNO_x production. HO_x amounts increase by 0.1 to 0.2 ppt as LNO_x production increases, since the primary source of HO_x, photolysis of O_3 followed by reaction of $O(^1D)$ with water vapor, is enhanced by the additional O_3. HO_x enhancements show correlation with changes in local flash rate, with the dependence being stronger over Africa and Southeast Asia and weaker over South America. Increasing LNO_x production leads to substantial decreases in the upper-tropospheric NO_2/NO ratio, particularly over South America and Africa, where the lightning-NO production is maximized. This, in turn, leads to decreases in the HO_2/OH ratio, as the increase in NO shifts the HO_2/OH equilibrium toward OH via the reaction of NO with HO_2. Local changes in the HO_2/OH ratio are moderately correlated with

local flash rate over South America but are uncorrelated over Africa and Southeast Asia.

4. Comparisons with observations

We compare model output from the CCM sensitivity simulations to several satellite data sets, including Ozone Monitoring Instrument (OMI) tropospheric NO_2 columns [*Bucsela et al.*, 2013], Tropospheric Emission Spectrometer (TES) level-2 O_3 [*Herman et al.*, 2012], OMI level-2 TCO [*Liu et al.*, 2010] and Ozone Monitoring Instrument/Microwave Limb Sounder (OMI/MLS) TCO [*Ziemke et al.*, 2006], as well as in situ O_3 profiles from the Southern Hemisphere ADitional OZonesondes (SHADOZ) data set [*Thompson et al.*, 2012].

Figures 7i (Western Hemisphere) and 7ii (Eastern Hemisphere) compare CCM tropospheric column NO_2 (panels a through e) to the OMI standard (OMIstd) tropospheric column NO_2 product (panel f). Averaging kernel (avK) information provided by OMI has been applied to the model output to ensure comparability of the two data sets; this has led to changes in mean column NO_2 of -6.7 % in the tropical Western Hemisphere and 0.0 % in the tropical Eastern Hemisphere for the baseline stdLNOx simulation (not shown). The CCM, in all cases, underestimates OMIstd NO_2, particularly over Brazil, northern Australia, southern Africa and the equatorial western Pacific; however, the spatial distribution of the NO_2 is reasonably well captured by the model. To clarify which CCM LNO_x scenario best reproduces the observed column NO_2, we calculate the root-mean-square error (RMSE), the centered root-mean-square error (RMSC) and the root-mean-square bias (RMSB) with respect to OMIstd tropospheric column NO_2 (Table 1). The small reduction in RMSC and the large reduction in RMSB going from .5xLNOx to stdLNOx is strong evidence that the stdLNOx source is more consistent with OMI than the .5xLNOx source. However, the small increase in RMSC and the large reduction in

RMSB going from stdLNOx to 2xLNOx suggests that a low bias in at least one additional NO_x source is contributing to the low bias in NO_2. Furthermore, after doubling the LNO_x source, the model is biased low in the Southern Hemisphere and biased high in the Northern Hemisphere, with the exception of eastern China, where anthropogenic emissions are likely underestimated. The Southern Hemisphere low bias is at least partially due to the low bias in model flashes over South America (south of 15°S) and over Africa (south of the equator), as shown in Figure A2. Since the dfLNOx flashes are based on OMI/MLS climatology rather than model dynamic parameters, the Southern Hemisphere bias for the dfLNOx simulation is smaller than it is for the stdLNOx simulation. Taking into consideration that model flashes are biased low over these regions, we believe that the stdLNOx source is most consistent with OMIstd tropospheric column NO_2.

Comparisons of the OMIstd NO_2 product to version 2 of the Dutch OMI NO_2 (DOMINO) product reveal that OMIstd exhibits a low mean bias of approximately -21 % over the tropics, with high biases (up to 85 %) occurring over a few localized regions. *Rivas et al.* [2014] observed a bias in OMI slant column densities; they believe that this bias does not affect tropospheric NO_2 columns, but does cause an overall OMI bias in stratospheric NO_2 of 0.6×10^{15} molecules cm^{-2}, 20 % relative to limb observations. However, Swartz et al. claim, through comparisons against independent observations and GMI CTM output, that the spectral fitting procedure used by both OMI NO_2 products causes a high bias of perhaps 15 to 35 % that affects both tropospheric and stratospheric vertical column densities (The impact of NO_2 slant column density retrieval bias on stratospheric and tropospheric vertical column densities, submitted to Geophysical Research Letters, 2014). Ongoing follow-up studies at KNMI and NASA-GSFC will determine whether OMI tropospheric NO_2 columns are indeed biased high and whether

some of the low bias the model is showing with respect to OMI is due to a high bias in the OMI data set.

Mean CCM O_3 biases are calculated with respect to TES O_3 data, after applying TES avK information to the model output. In general, positive model biases are more prevalent in the UT (Figure 8i) and negative biases are predominant in the LT (Figure 8ii). The .5xLNOx run has the smallest overall bias in the Western Hemisphere UT (-12.9 %) and the stdLNOx run has the smallest bias in the Eastern Hemisphere UT (+10.4 %). Localized biases exceeding 15 % can be seen throughout much of the tropical and subtropical Southern Hemisphere UT in the stdLNOx and 2xLNOx runs. In the LT, stdLNOx has the lowest bias in the Western Hemisphere (-6.9 %) and 2xLNOx has the lowest bias in the Eastern Hemisphere (-4.1 %). Comparisons of TES data to several ozonesonde data sets [*Herman et al.*, 2012] reveal a positive mean bias of up to 10 % in the lower and middle troposphere, and a near-zero mean bias near 200 hPa, when averaged over 15°N to 15°S (276 coincident TES-sonde measurements). Thus, a small low bias in lower-tropospheric TES O_3 is a possible contributor to the low bias in lower-tropospheric model O_3.

Model simulations are also compared to OMI (Figure 9) and OMI/MLS (Figure 10) TCO products. OMI is provided on the model's native 2° × 2.5° grid; OMI/MLS is initially provided on a finer 1° × 1.25° grid, but is re-gridded to the coarser model resolution by aggregating adjacent grid boxes. The difference in mean tropical TCO between OMI and OMI/MLS is 0.77 Dobson Units (DU), approximately 2.6 %, showing reasonable agreement between the two data sets. The .5xLNOx run shows the smallest bias in mean tropical TCO with respect to both OMI (-1 %) and OMI/MLS (-4 %). All other simulations (with the exception of noLNOx) show small to moderate positive biases, ranging from 7.3 to 28.6 % (Figure 9b-e; Figure 10a-d). Discrepancies in model output between Figures 9 and 10 are due to the fact that avK information

is provided with the OMI data set, but not with OMI/MLS; therefore, CCM output is avK-adjusted in Figure 9, but is unadjusted in Figure 10. Comparisons of model output both with and without the avK applied indicate that avK adjustment has a relatively small impact on TCO.

SHADOZ ozonesonde data are used to compare the vertical O_3 profiles modeled by the four sensitivity simulations. Figure 11 shows CCM and SHADOZ mean O_3 profiles for four SHADOZ sites: Pago Pago, American Samoa; Ascension Island; San Cristobal, Galapagos; and La Réunion Island. These locations are chosen because they have at least 10 days of SHADOZ ozonesonde data during the SON 2007 time period. Mean CCM O_3 profiles are calculated using model output from only those dates with coincident SHADOZ launches (see Figure 11 caption), and at the CCM output times nearest to the times of launch. In general, the stdLNOx profiles are biased low with respect to SHADOZ in the middle and upper troposphere. This low bias is most noticeable at Ascension Island, where the 2xLNOx profiles agree best with the observed profile. The low bias at Ascension Island is most likely due to a low bias in modeled flash rates over central Africa (see Figure A1), as the shape of the observed and 2xLNOx profiles agree well. The stdLNOx model profiles agree best with SHADOZ at Pago Pago and San Cristobal, although the stdLNOx profile at Pago Pago is biased high in the LT and biased low in the UT.

In order to address the inconsistencies between the CCM-TES and CCM-SHADOZ comparisons, we perform a direct comparison of the two data sets. TES O_3 columns are calculated by extracting TES profiles at the grid point nearest to each SHADOZ site location (TES_{SHADOZ}), and then averaging over the days during which SHADOZ launches occurred (see Figure 11 caption). The distance between each SHADOZ location and its nearest TES profile ranges between 65 and 136 km. TES data are not available on 28 November and, consequently, the mean TES profiles calculated for both Ascension Island and La Réunion Island include one

less day than the mean SHADOZ profiles. Table 2 lists the TCO values for the four SHADOZ sites considered in this study, as calculated by the GEOS-5 CCM, by SHADOZ and by TES. Biases between TES and SHADOZ TCO are small, varying from -15 % at Pago Pago, American Samoa to +7.4 % at San Cristobal, Galapagos. In order to determine whether the days with SHADOZ profiles can adequately portray the entire SON 2007 time period, we calculate the mean TES column using all available TES days during SON 2007 (TES_{ALL}). For all four locations, TES_{SHADOZ} is within 7 DU of TES_{ALL} and SHADOZ is within 5 DU of TES_{ALL}. This suggests that SHADOZ ozonesonde data, although limited, can provide a reliable representation of the mean SON 2007 O_3 profile. Overall, the stdLNOx simulation is biased high with respect to SHADOZ and TES_{SHADOZ} TCO at Pago Pago, and low with respect to SHADOZ and TES_{SHADOZ} TCO at Ascension Island. Biases in mean TCO for the stdLNOx simulation at San Cristobal and La Réunion are minor.

The inconsistencies in the agreement from model to observations and between observations underline our need to (a) better resolve regional variations in flash rate and NO production per flash, and (b) understand, and correct for, biases in the observational data sets.

5. Significance of LNO_x to natural radiative forcing

NO_x serves as a catalyst to O_3 production and, therefore, plays a role in short-term atmospheric warming. Conversely, NO_x also influences OH formation, subsequently reducing CH_4 and leading to short-term radiative cooling [*Kunhikrishnan and Lawrence*, 2004; *Martini et al.*, 2011]; however, due to the short length of our simulations relative to the lifetime of CH_4 (approximately 9 years), we neglect this cooling effect in our study.

Radiative forcing is defined in this study as the net flux imbalance at the tropopause; therefore, measured flux changes either into or out of the troposphere are considered to contribute to changes in overall atmospheric radiative forcing. Figure 12 depicts the mean net radiative flux near the tropopause (CCM pressure level 163 hPa) that is attributable only to lightning-produced O_3, which is calculated by subtracting the net flux in the noLNOx simulation from the net flux in the .5xLNOx, stdLNOx, dfLNOx and 2xLNOx simulations. Halving and doubling the LNO_x production cause changes in total radiative flux in the tropics of -43 and +63 %, respectively. Localized flux maxima, which range from 0.30 to 0.45 W m^{-2} (.5xLNOx) to greater than 1.20 W m^{-2} (2xLNOx), are evident off the eastern coast of Brazil, over southern Africa and over northern Australia. Increasing the LNO_x source strength by a factor of 4 (2.5 to 10 Tg N a^{-1}) leads to an approximately 188 % increase in net radiative flux near the tropopause.

The difference in radiative flux between the stdLNOx and dfLNOx simulations (0.46 W m^2 versus 0.53 W m^2) is due to the differences in the altitude and distribution of the LNO_x production. Although both simulations have the same total source strength, they each apply different algorithms to partition the emissions in the horizontal and the vertical. The stdLNOx parameterization produces a strong pulse of NO_x between 7 and 10 km, which is co-located with model deep convection, whereas the dfLNOx simulation gradually releases NO_x over a broader peak between 9 and 14 km, which is consistent with the climatological distribution of flashes but does not necessarily coincide with model convection. The radiative forcing over Africa is larger in the dfLNOx run than in the stdLNOx run, most likely because the dfLNOx run has higher flash rates and greater LNO_x production than the stdLNOx run, which tends to underestimate flash rates over this region. Findings from *Labrador et al.* [2005] show that the global NO_x burden is highly dependent on both the vertical placement and the source strength of lightning-

produced NO_x; Figure 12 suggests that an inaccurate representation of either may have significant implications with respect to atmospheric radiative forcing.

6. Discussion and Summary

The flash rate parameterization employed in the GEOS-5 CCM used for this study aims to produce flashes that coincide with modeled convection. While, in some cases, this might lead to inaccuracies with respect to reproducing the distribution or rate of climatologically-observed flashes, we believe that we are taking a step in the right direction by maintaining consistency between the lightning flashes and the dynamics that drive them.

The LNO_x sensitivity simulations used in this study show that a factor-of-four increase in lightning NO production (125 to 500 moles per flash) significantly impacts the chemical composition of the tropical troposphere. These effects are maximized in regions of peak LNO_x production, but are also observed throughout the middle and upper troposphere and, in some cases, well into the PBL. In order to determine which LNO_x production scenario best agrees with current observations, we compare model output from the four sensitivity simulations to various satellite and in situ data products. Both the stdLNOx and dfLNOx simulations exhibit negative biases in mean tropical tropospheric column NO_2 of approximately -30 and -25 %, respectively, when compared to OMIstd. Initially, this suggests that applying a global LNO_x production rate of 250 moles per flash is too low. However, further investigation suggests that underestimated flash rates over South America and Africa, as well as a low bias in at least one additional source of atmospheric NO_x, may be contributing to the low bias in tropospheric column NO_2. Both stdLNOx and dfLNOx show high biases with respect to observed TCO (OMI and OMI/MLS), averaging approximately 9 and 13 %, respectively. The .5xLNOx runs

compares well against observed TCO, reasonably capturing the magnitude and distribution of the observed O_3 columns, but it vastly underestimates column NO_2, particularly over Brazil, southern Africa, Australia and Southeast Asia. The 2xLNOx run exhibits the smallest bias in mean tropospheric column NO_2, but also the largest bias in satellite-derived TCO. Overall, comparisons with observations indicate that a 5.0 Tg N a^{-1} source is best, as a 2.5 Tg N a^{-1} source underestimates tropospheric columns of NO_2, while a 10 Tg N a^{-1} source overestimates tropospheric columns of O_3. In all cases, the noLNOx simulation reveals an unrealistic representation of both the satellite and in situ tropospheric observations.

Biases in modeled LNO_x, due to regional biases in modeled flashes and/or regional differences in NO production per flash, add uncertainty to this analysis. Currently, we are faced with the conundrum that increasing the LNO_x source strength to reduce the low biases in tropospheric column NO_2 will likely exacerbate the already high biases in column O_3. Underestimations in non-lightning NO_x source emissions may be partially to blame for this conundrum, but may also be due to inherent biases in the satellite data and/or inaccuracies in model chemistry, such as underestimations of the upper-tropospheric NO_x lifetime or overestimations of the O_3 production rate. Overall, further research into (a) investigating potential improvements in the structure and operation of the CCM chemical mechanism, and (b) the application of additional meteorological and surface parameters for improving the lightning parameterization, in combination with improved observational data sets, should improve our ability to accurately model the distribution of flashes, the production of NO per flash, and the impact on atmospheric chemistry.

Acknowledgements. The data used for the results of this paper are available from the author upon request. This work was supported by NASA Modeling and Analysis Program grant NASA/NNX09AJ37G. I would like to thank Dale Allen and Ken Pickering for their advice and continuous support.

Appendices

Appendix I. Chemistry-Climate Model: Replay Mode

The GEOS-5 CCM used for this experiment is run in "replay mode", utilizing the Modern-Era Retrospective analysis for Research and Applications (MERRA) reanalysis data [*Rienecker et al.*, 2011] to constrain the atmospheric dynamics in the CCM. The analysis is implemented at 0.67° longitude by 0.5° latitude horizontal resolution, with 72 levels and a model top of 0.01 hPa, and is re-gridded online to CCM resolution within replay mode. Surface data, near surface meteorology, selected upper-air levels, and vertically-integrated fluxes and budgets are produced at one-hour intervals. MERRA uses the Incremental Analysis Update (IAU) technique developed by *Bloom et al.* [1996] to minimize spurious periodic perturbations of the analysis.

Replay mode can be executed in any of three different options: Exact, Regular and Intermittent. For this study we employ the 'Regular' replay mode, which replays to an existing analysis by simulating the IAU process (IAU = assimilated analysis – model forecast), i.e., it creates a new forcing. Hour-3 files are used, since they contain the previous full analysis increment and are well balanced. Regular replay reads in the analyzed fields every six hours and then re-computes the analysis 'increments' to update the meteorology every 30 minutes. Convective and diffusive transports are also recomputed every 30 minutes. Note that the chemistry calculations within the CCM have no feedback on the meteorology. The analysis does not generally modify the stratosphere, and basically relaxes itself to the background. However, the lower levels are left in a generally unbalanced state which, upon re-insertion into the model, can produce gravity wave instabilities that propagate into the stratosphere. To prevent the development of gravity wave instabilities in the upper layers of the model, the IAU increment is

linearly damped in the stratosphere between two specified pressure levels. Since the meteorological fields are ingested exactly as they have been archived, we are essentially eliminating the need for reprocessing or reformatting the data. This allows us to perform and reproduce global simulations in significantly less time, making using replay mode more efficient than using the GMI CTM alone.

Appendix II. Lightning parameterization

Flash rates are correlated with numerous meteorological variables including surface temperature [*Price*, 1993; *Williams and Stanfill*, 2002; *Markson*, 2007], convective available potential energy (CAPE) [*Rutledge et al.*, 1992], cloud top height [*Price and Rind*, 1992; *Price et al.*, 1997], cold-cloud depth [*Futyan and Del Genio*, 2007; *Yoshida et al.*, 2009], convective precipitation [*Meijer et al.*, 2001], upper-tropospheric convective mass flux [*Allen and Pickering*, 2002], integrated convective mass flux [*Deierling et al.*, 2005], updraft vertical velocity or volume [*Deierling and Peterson*, 2008; *Barthe et al.*, 2010], precipitation ice mass, path, or flux [*Petersen et al.*, 2005; *Deierling et al.*, 2008; *Barthe et al.*, 2010], and aerosol concentrations [*Michalon et al.*, 1999; *Andreae et al.*, 2004; *Altaratz et al.*, 2010; *Yuan et al.*, 2011].

The GEOS-5 GCM was run in a free running mode for a five-year time period (1994 to 1998), archiving every three hours the meteorological fields needed to calculate 19 variables related to flash rate. A multivariable regression was then used to determine which combination of variables explained the most variance in "daily" average climatological flash rates from version 2.2 of the Optical Transient Detector/Lightning Imaging Sensor (OTD/LIS) [*Cecil et al.*, 2014]. Due to sampling constraints, these "daily" OTD/LIS values are 98-day centered averages.

Separate regressions were performed over land (more than 50 % land-covered) and ocean grid boxes, using grid boxes and times where the model showed deep convection (i.e., model cloud tops of less than 500 hPa and non-zero convective precipitation rates). The resulting analysis showed that a combination of five variables explained the most variance: (1) cold-cloud depth, (2) total cloud depth, (3) CAPE, (4) integrated cold-cloud (less than 263 K) convective mass flux, and (5) the cube of the perturbation of surface temperature (T_{sfc}) from a reference temperature (in this case 273 K). For unit consistency, each of the variables was divided by its five-year mean (4.36, 9.27, 34.4, 21.4 and 14600, respectively) before the fits were performed. To minimize the impact of extreme events on the fit, each of the normalized variables was constrained to be between 0 and 3. The resulting equation is:

$$Y = a_1X_1 + a_2X_2 + a_3X_3 + a_4X_4 + a_5X_5, \qquad \text{(A1)}$$

where X_1 = normalized cold-cloud depth, X_2 = normalized total cloud depth, X_3 = normalized CAPE, X_4 = normalized integrated cold-core convective mass flux, and X_5 = normalized $(T_{sfc} - 273\ K)^3$ for T_{sfc} greater than 273 K and 0 for T_{sfc} less than 273 K.

The fitting coefficients (a_1, a_2, a_3, a_4, and a_5) were determined separately for marine and continental locations. The regression analysis that selected these five variables was performed separately for tropical marine, tropical continental, extratropical marine, and extratropical continental locations. When the tropical and extratropical fits were combined, it was determined that a simpler formula, which incorporated only X_4 and X_5, performed nearly as well as the five-variable equation. This expression goes as follows:

$$Y = a\,(X_4 + X_5), \qquad \text{(A2)}$$

where a was set to 0.003 at marine locations and 0.053 at continental locations, producing a global flash rate of 46 flashes per second and providing a reasonable partitioning of flashes

between continental and marine locations. Grid boxes adjacent to land grid boxes were defined as continental in character, while the remaining water grid boxes were defined as marine. The desired LNO_x production rates of 0, 2.5, 5.0 and 10 Tg N a^{-1} were obtained for this study by multiplying the flash rate by 0, 150, 250 and 500 moles per flash, respectively. Vertical distributions from *Ott et al.* [2010] are used to distribute the lightning NO in the vertical.

Currently, the five-variable parameterization is the standard scheme used in the NASA GEOS-5 CCM, but for this study the more concise two-variable parameterization is used. This simpler expression not only lessens the possibility of over-fitting, but also works nearly as well as the five-term expression due to a high level of correlation between the "independent" variables. For example, the cube of the surface temperature at locations with deep convection is correlated with CAPE, and the integrated cold-core convective mass incorporates cold-cloud depth during the integration. The two-parameter version of the parameterization was tested using the Fortuna 2.5 version of the GEOS-5 CCM for a two-year simulation beginning in February 1997. Figure A1 compares seasonal model flash rates from this simulation with observed flash rates from OTD/LIS. Overall, flash rates are reasonable, although the model substantially overestimates Brazilian flash rates (especially in MAM) and underestimates central African flash rates. The model also underestimates flash rates downwind of continents and overestimates flash rates at relatively remote tropical marine locations. These biases exist because the transition from continental convection to marine convection is more gradual than implied by the continental/marine flags used in the parameterization.

The differences between modeled and observed flash rates can be attributed to several factors, including (1) errors in the climatological location and strength of model deep convection, (2) errors introduced by the assumption that the relationship between flash rates and deep

convection can be explained by our simple formula, and (3) errors introduced by the comparison of observed flash rates from one time period with modeled flash rates from another time period. The flash energy associated with cloud-to-ground (CG) and inter-cloud (IC) flashes has been the subject of much recent research. Recent midlatitude and subtropical storm-scale case studies, involving cloud-resolved models constrained by observed flash rates and anvil NO_x measurements from field experiments, such as STERAO [*DeCaria et al.*, 2000, 2005], CRYSTAL-FACE [*Ott et al.*, 2010] and EULINOX [*Fehr et al.*, 2004; *Ott et al.*, 2007], have found that IC flashes are nearly as energetic as CG flashes (see also *Ridley et al.*, 2005) and that both CG and IC midlatitude flashes produce, on average, 500 moles of N per flash [*Ott et al.*, 2010]. Recent laboratory work by *Cooray et al.* [2009] also suggests that on average NO production by an IC flash is approximately equivalent to that of a CG flash. The 500-moles-per-flash value for midlatitude flashes is on the higher end of estimates by *Schumann and Huntrieser* [2007], and is much higher than a recent top-down estimate by *Beirle et al.* [2010] based on observed flash rates and NO_2 columns from SCIAMACHY. Figure A2 compares mean OTD/LIS flash rates to model flashes calculated using MERRA meteorological fields for the SON 2007 time period used in this study. In general, the distribution is similar to the climatological SON distribution shown in A1, with both plots showing low biases over central Africa. These biases influence modeled atmospheric composition over central Africa and the Atlantic, as shown in *Allen and Pickering* [2002] and *Allen et al.* [2010], and in the main body of this article.

References

Allen, D. J., and K. E. Pickering (2002), Evaluation of lightning flash rate parameterizations for use in a global chemical transport model, *J. Geophys. Res*., *107*(D23), 4711, doi:10.1029/2002JD002066.

Allen, D. J., J. E. Dibb, B. Ridley, K. E. Pickering, and R. W. Talbot (2003), An estimate of the stratospheric contribution to springtime tropospheric ozone maxima using TOPSE measurements and beryllium-7 simulations, *J. Geophys. Res, 108*(D4), 8355, doi:10.1029/2001JD001428.

Allen, D. J., K. Pickering, B. Duncan, and M. Damon (2010), Impact of lightning-NO emissions on North American photochemistry as determined using the Global Modeling Initiative (GMI) model, *J. Geophys. Res.*, *115*, D22301, doi:10.1029/2010JD014062.

Allen, D. J., K. E. Pickering, R. W. Pinder, B. H. Henderson, K. W. Appel, and A. Prados (2012), Impact of lightning-NO on eastern United States photochemistry during the summer of 2006 as determined using the CMAQ model, *Atmos. Chem. Phys*., *12*, 1737–1758, doi:10.5194/acp-12-1737-2012.

Altaratz, O., I. Koren, Y. Yair, and C. Price (2010), Lightning response to smoke from Amazonian fires. *Geophys. Res. Lett.*, *37*, L07801, doi:10.1029/2010GL042679.

Andreae, M. O., D. Rosenfeld, P. Artaxo, A. A. Costa, G. P. Frank, K. M. Longo, and M. A. F. Silva Dias (2004), Smoking rain clouds over the Amazon, *Science*, *303*(5662), 1337-1342, doi:10.1126/science.1092779.

Barthe, C., W. Deierling, and M. C. Barth (2010), Estimation of total lightning from various storm parameters: A cloud-resolving model study, *J. Geophys. Res.*, *115*, D24202, doi:10.1029/2010JD014405.

Beirle, S., U. Platt, M. Wenig, and T. Wagner (2004), NO_x production by lightning estimated with GOME, *Adv. Space Res.*, *34*(4), 793-797, doi:10.1016/j.asr.2003.07.069.

Beirle, S., N. Spichtinger, A. Stohl, K. L. Cummins, T. Turner, D. Boccippio, O. R. Cooper, M. Wenig, M. Grzegorski, U. Platt, and T. Wagner (2006), Estimating the NO_x produced by lightning from GOME and NLDN data: a case study in the Gulf of Mexico, *Atmos. Chem. Phys.*, *6*, 1075-1089, doi:10.5194/acp-6-1075-2006.

Beirle, S., H. Huntrieser, and T. Wagner (2010), Direct satellite observations of lightning-produced NO_x, *Atmos. Chem. Phys.*, *10*, 10965-10986, doi:10.5194/acp-10-10965-2010.

Bloom, S. C., L. L. Takacs, A. M. da Silva, and D. Ledvina (1996), Data Assimilation Using Incremental Analysis Updates, *Mon. Wea. Rev.*, *124*(6), 1256-1271, doi:10.1175/1520-0493(1996)124.

Boccippio, D. J., W. Koshak, R. Blakeslee, K. Driscoll, D. Mach, D. Buechler, W. Boeck, H. J. Christian, S. J. Goodman (2000), The Optical Transient Detector (OTD): Instrument Characteristics and Cross-Sensor Validation, *J. Atmos. Oceanic Technol.*, *17*(4), 441-458, doi:10.1175/1520-0426(2000)017.

Boccippio, D. J., W. Koshak, and R. J. Blakeslee (2002), Performance Assessment of the Optical Transient Detector and Lightning Imaging Sensor Part I: Predicted Diurnal Variability, *J. Atmos. Oceanic Technol.*, *19*(9), 1318-1332, doi:10.1175/1520-0426(2002)019.

Bond, D. W., S. Steiger, R. Zhang, X. Tie, and R. E. Orville (2002), The importance of NO_x production by lightning in the tropics, *Atmos. Env.*, *36*(9), 1509-1519, doi:10.1016/51352-2310(01)00553-2.

Bucsela, E. J., et al. (2010), Lightning-generated NO_x seen by the Ozone Monitoring Instrument during NASA's Tropical Composition, Cloud and Climate Coupling Experiment (TC^4), *J. Geophys. Res.*, *115*, D00J10, doi:10.1029/2009JD013118.

Bucsela, E. J., N. A. Krotkov, E. A. Celarier, L. N. Lamsal, W. H. Swartz, P. K. Bhartia, K. F. Boersma, J. P Veefkind, J. F. Gleason, and K. E. Pickering (2013), A new stratospheric and tropospheric NO_2 retrieval algorithm for nadir-viewing satellite instruments: applications to OMI, *Atmos. Meas. Tech.*, *6*, 2607-2626, doi:10.5194/amt-6-2607-2013.

Cecil, D. J., D. E. Buechler, and R. J. Blakeslee (2014), Gridded lightning climatology from TRMM-LIS and OTD: Dataset description, *Atmos. Res.*, *135-136*, 404-414, doi:10.1016/j.atmosres.2012.06.028.

Chandra, S., J. R. Ziemke, X. Tie, and G. Brasseur (2004), Elevated ozone in the troposphere over the Atlantic and Pacific oceans in the Northern Hemisphere, *Geophys. Res. Lett*., *31*, L23102, doi:10.1029/2004GL020821.

Christian, H. J., et al. (2003), Global frequency and distribution of lightning as obsered from space by the Optical Transient Detector, *J. Geophys. Res.*, *108*(D1), 4005, doi:10.1029/2002JD002347.

Cooper, O. R., et al. (2006), Large upper tropospheric ozone enhancements above midlatitude North America during summer: In situ evidence from the IONS and MOZAIC ozone measurement network, *J. Geophys. Res.*, *111*, D24S05, doi:10.1029/2006JD007306.

Cooper, O. R., et al. (2007), Evidence for a recurring eastern North America upper tropospheric ozone maximum during summer, *J. Geophys. Res.*, *112*, D23304, doi:10.1029/2007JD008710.

Cooray V., M. Rahman, and V. Rakov (2009), On the NO_x production by laboratory electrical discharges and lightning, *J. Atmos. Sol. Terr. Phys.*, *71*(17-18), 1877-1889, doi:10.1016/j.jastp.2009.07.009.

Cummings, K. A., T. L. Huntemann, K. E. Pickering, M. C. Barth, W. C. Skamarock, H. Höller, H.-D. Betz, A. Volz-Thomas, and H. Schlager (2013), Cloud-resolving chemistry simulation of a Hector thunderstorm, *Atmos. Chem. Phys.*, *13*, 2757-2777, doi:10.5194/acp-13-2757-2013.

Dahlmann, K., V. Grewe, M. Ponater, and S. Matthes (2011), Quantifying the contributions of individual NO_x sources to the trend in ozone radiative forcing, *Atm. Env.*, *45*, 2860-2868, doi:10.1016/j.atmosenv.2011.02.071.

DeCaria, A. J., K. E. Pickering, G. L. Stenchikov, J. R. Scala, J. L. Stith, J. E. Dye, B. A. Ridley, and P. Laroche (2000), A cloud-scale model study of lightning-generated NO_x in an individual thunderstorm during STERAO-A, *J. Geophys. Res.*, *105*(D9), 11601-11616.

DeCaria, A. J., K. E. Pickering, G. L. Stenchikov, and L. E. Ott (2005), Lightning-generated NO_x and its impact on tropospheric ozone production: A three-dimensional modeling study of a Stratosphere-Troposphere Experiment: Radiation, Aerosols and Ozone (STERAO-A) thunderstorm, *J. Geophys. Res.*, *110*, D14303, doi:10.1029/2004JD005556.

Deierling, W., and W. A. Petersen (2008), Total lightning activity as an indicator of updraft characteristics, *J. Geophys. Res.*, *113*, D16210, doi:10.1029/2007JD009598.

Deierling, W., J. Latham, W. A. Petersen, S. M. Ellis, and H. J. Christian Jr. (2005), On the relationship of thunderstorm ice hydrometeor characteristics and total lightning measurements, *Atmos. Res.*, *76*, 114-126, doi:10.1016/j.atmosres.2004.11.023.

Deierling, W., W. A. Peterson, J. Latham, S. Ellis, and H. J. Christian (2008), The relationship between lightning activity and ice fluxes in thunderstorms, *J. Geophys. Res.*, *113*, D15210, doi:10.1029/2007JD009700.

Dentener, F. J. and P. J. Crutzen (1993), Reaction of N_2O_5 on tropospheric aerosols: Impact on the global distributions of NO_x, O_3, and OH, *J. Geophys. Res.*, *98*(D4), 7149-7163, doi:10.1029/92JD02979.

Duncan, B. N., S. E. Strahan, Y. Yoshida, S. D. Steenrod, and N. Livesey (2007), Model study of the cross-tropopause transport of biomass burning pollution, *Atmos. Chem. Phys.*, *7*, 3713-3736, doi:10.5194/acp-7-3713-2007.

Fehr, T., H. Höller, and H. Huntrieser (2004), Model study on production and transport of lightning-produced NO_x in a EULINOX supercell storm, *J. Geophys. Res.*, *109*, D09102, doi:10.1029/2003JD003935.

Futyan, J. M., and A. D. Del Genio (2007), Relationships between lightning and properties of convective cloud clusters, *Geophys. Res. Lett*., *34*, L15705, doi:10.1029/2007GL030227.

Herman, R., and G. Osterman (editors), C. Boxe, K. Bowman, K. Cady-Pereira, T. Clough, A. Eldering, B. Fisher, D. Fu, R. Herman, D. Jacob, L. Jourdain, S. Kulawik, M. Lampel, Q. Li, J. Logan, M. Luo, I. Megretskaia, R. Nassar, G. Osterman, S. Paradise, V. Payne, H. Revercomb, N. Richards, M. Shephard, D. Tobin, S. Turquety, F. Vilnrotter, K. Wecht, H. Worden, J. Worden, and L. Zhang (2012), Earth Observing System (EOS) Tropospheric Emission Spectrometer (TES) Data Validation Report (Version F06_08, F06_09 data), Version 5.0, JPL Internal Report D-33192, Jet Propul. Lab., Pasadena, Calif., April 8, 2012.

Huntrieser, H., U. Schumann, H. Schlager, H. Höller, A. Giez, H.-D. Betz, D. Brunner, C. Forster, O. Pinto Jr., and R. Calheiros (2008), Lightning activity in Brazilian thunderstorms

during TROCCINOX: implications for NO_x production, *Atmos. Chem. Phys., 8*, 921–953, doi:10.5194/acp-8-921-2008.

Huntrieser, H., H. Schlager, M. Lichtenstern, A. Roiger, P. Stock, A. Minikin, H. Höller, K. Schmidt, H.-D. Betz, G. Allen, S. Viciani, A. Ulanovsky, F. Ravegnani, and D. Brunner (2009), NO_x production by lightning in Hector: first airborne measurements during SCOUT-O3/ACTIVE, *Atmos. Chem. Phys.*, *9*, 8377-8412, doi:10.5194/acp-9-8377-2009.

Huntrieser, H., H. Schlager, M. Lichtenstern, P. Stock, T. Hamburger, H. Höller, K. Schmidt, H.-D. Betz, A. Ulanovsky, and F. Ravegnani (2011), Mesoscale convective systems observed during AMMA and their impact on the NO_x and O_3 budget over West Africa, *Atmos. Chem. Phys.*, *11*, 2503-2536, doi:10.5194/acp-11-2503-2011.

Jacob, D. J. (1999), *Introduction to Atmospheric Chemistry*, vol. xii, 266 pp., Princeton Univ. Press, Princeton, N.J..

Jing, P., D. M. Cunnold, E.-S. Yang, H.-J. Wang (2005), Influence of isentropic transport on seasonal ozone variations in the lower stratosphere and subtropical upper troposphere, *J. Geophys. Res.*, *110*, D10110, doi:10.1029/2004JD005416.

Jourdain, L., and D. A. Hauglustaine (2001), The Global Distribution of Lightning NO_x Simulated on-line in a General Circulation Model, *Phys. Chem. Earth*, *26*(8), 585-591.

Koshak, W., H. Peterson, A. Biazar, M. Khan, and L. Wang (2014): The NASA Lightning Nitrogen $O_x$ides Model (LNOM): Application to air quality modeling, *Atmos. Res.*, *135-136*, 363-369, doi:10.1016/j.atmosres.2012.12.015.

Kunhikrishnan, T. and M. G. Lawrence (2004), Sensitivity of NO_x over the Indian Ocean to emissions from the surrounding continents and nonlinearities in atmospheric chemistry responses, *Geophys. Res. Lett.*, *31*, L15109, doi:10.1029/2004GL020210.

Labrador, L. J., R. von Kuhlmann, and M. G. Lawrence (2005), The effects of lightning-produced NO_x and its vertical distribution on atmospheric chemistry: sensitivity simulations with MATCH-MPIC, *Atmos. Chem. Phys.*, *5*, 1815-1834, doi:10.5194/acp-5-1815-2005..

Lacis, A. A., D. J. Wuebbles, and J. A. Logan (1990), Radiative forcing of climate by changes in the vertical distribution of ozone, *J. Geophys. Res.*, *95*(D7), 9971-9981, doi:10.1029/JD095iD07p09971.

Liu, X., P. K. Bhartia, K. Chance, R. J. D. Spurr, and T. P. Kurosu (2010), Ozone profile retrievals from the Ozone Monitoring Instrument, *Atmos. Chem. Phys.*, *10*, 2521-2537, doi:10.5194/acp-10-2521-2010.

Mach, D. M., H. J. Christian, R. J. Blakeslee, D. J. Boccippio, S. J. Goodman, and W. L. Boeck (2007), Performance assessment of the Optical Transient Detector and Lightning Imaging Sensor, *J. Geophys. Res.*, *112*, D09210, doi:10.1029/2006JD007787.

Markson, R. (2007), The Global Circuit Intensity: Its Measurement and Variation over the Last 50 Years, *Bull. Am. Meteorol. Soc*., *88*(2), 223-241, doi:10.1175/BAMS-88-2-223.

Martin, R. V., D. J. Jacob, J. A. Logan, J. M. Ziemke, and R. Washington (2000), Detection of a lightning influence on tropical tropospheric ozone, *Geophys. Res. Lett*., *27*(11), 1639-1642, doi:10.1029/1999GL011181.

Martin, R. V., B. Sauvage, I. Folkins, C. E. Sioris, C. Boone, P. Bernath, and J. Ziemke (2007), Space-based constraints on the production of nitric oxide by lightning, *J. Geophys. Res.*, *112*, D09309, doi:10.1029/2006JD007831.

Martini, M., D. J. Allen, K. E. Pickering, G. L. Stenchikov, A. Richter, E. J. Hyer, and C. P. Loughner (2011), The impact of North American anthropogenic emissions and lightning on

long-range transport of trace gases and their export from the continent during summers 2002 and 2004, *J. Geophys. Res*., *116*, D07305, doi:10.1029/2010JD014305.

Meijer, E. W., P. F. J. van Velthoven, D. W. Brunner, H. Huntrieser, and H. Kelder (2001), Improvement and Evaluation of the Parameterisation of Nitrogen Oxide Production by Lightning, *Phys. Chem. Earth*, *26*(8), 577-583.

Michalon, N., A. Nassif, T. Saouri, J. F. Royer, and C. A. Pontikis (1999), Contribution to the climatological study of lightning, *Geophys. Res. Lett*., *26*(20), 3097-3100, doi:10.1029/1999GL010837.

Ott, L. E., K. E. Pickering, G. L. Stenchikov, H. Huntrieser, and U. Schumann (2007), Effects of lightning NO_x production during the 21 July European Lightning Nitrogen Oxides Project storm studied with a three-dimensional cloud-scale chemical transport model, *J. Geophys. Res.*, *112*, D05307, doi:10.1029/2006JD007365.

Ott, L. E., K. E. Pickering, G. L. Stenchikov, D. J. Allen, A. J. Decaria, B. Ridley, R.-F. Lin, S. Lang, and W.-K. Tao (2010), Production of lightning NO_x and its vertical distribution calculated from three-dimensional cloud-scale chemical transport model simulations. *J Geophys Res.*,*115*, D04301, doi:10.1029/2009JD011880.

Petersen, W. A., H. J. Christian, and S. A. Rutledge (2005), TRMM observations of the global relationship between ice water content and lightning, *Geophys. Res. Lett*., *32*, L14819, doi:10.1029/2005GL023236.

Pickering, K. E., Y. Wang, W.-K. Tao, C. Price, and J.-F. Mueller (1998), Vertical distributions of lightning NO_x for use in regional and global chemical transport models, *J. Geophys. Res.*, *103*(D23), 31203-31216, doi:10.1029/98JD02651.

Price, C. (1993), Global surface temperatures and the atmospheric electrical circuit, *Geophys. Res. Lett.*, *20*(13), 1363-1366, doi:10.1029/93GL01774.

Price, C., and D. Rind (1992), A simple lightning parameterization for calculating global lightning distributions, *J. Geophys. Res.*, *97*(D9), 9919-9933, doi:10.1029/92JD00719.

Price, C., J. Penner, and M. Prather (1997), NO_x from lightning, 1. Global distribution based on lightning physics, *J. Geophys. Res.*, *102*(D5), 5929-5941.

Ridley, B. A., K. E. Pickering, and J. E. Dye (2005), Comments on the parameterization of lightning-produced NO in global chemistry-transport models, *Atmos. Env.*, *39*(33), 6184-6187, doi:10.1016/j.atmosenv.2005.06.054.

Rienecker, M. M., et al. (2011), MERRA: NASA's Modern-Era Retrospective Analysis for Research and Applications, *J. Clim.*, *24*(14), 3624-3648, doi:10.1175/JCLI-D-11-00015.1.

Rivas, M. B., P. Veefkind, F. Boersma, P. Levelt, H. Eskes, and J. Gille (2014), Intercomparison of daytime stratospheric NO_2 satellite retrievals and model simulations, *Atmos. Meas. Tech. Discuss.*, *7*(1), 895-948, doi:10.5194/amtd-7-895-2014.

Rutledge, S. A., E. R. Williams, and T. D. Keenan (1992), The Down Under Doppler and Electricity Experiment (DUNDEE): Overview and Preliminary Results, *Bull. Am. Meteorol. Soc.*, *73*(1), 3-16, doi:10.1175/1520-0477(1992)073.

Schumann, U., and H. Huntrieser (2007), The global lightning-induced nitrogen oxides source, *Atmos. Chem. Phys.*, *7*, 3823-3907, doi:10.5194/acp-7-3823-2007.

Staudt, A. C., D. J. Jacob, F. Ravetta, J. A. Logan, D. Bachiochi, T. N. Krishnamurti, S. Sandholm, B. Ridley, H. B. Singh, and B. Talbot (2003), Sources and chemistry of nitrogen oxides over the tropical Pacific, *J. Geophys. Res.*, *108*(D2), 8239, doi:10.1029/2002JD002139.

Stockwell, D. Z., C. Giannakopoulos, P.-H. Plantevin, G. D. Carver, M. P. Chipperfield, K. S. Law, J. A. Pyle, D. E. Shallcross, K.-Y. Wang (1999), Modelling NO_x from lightning and its impact on global chemical fields, *Atmos. Env*., *33*, 4477-4493.

Thompson, A. M., et al. (2012), Southern Hemisphere Additional Ozonesondes (SHADOZ) ozone climatology (2005–2009): Tropospheric and tropical tropopause layer (TTL) profiles with comparisons to OMI-based ozone products, *J. Geophys. Res.*, *117*, D23301, doi:10.1029/2011JD016911.

van der Werf, G. R., J. T. Randerson, L. Giglio, G. J. Collatz, M. Mu, P. S. Kasibhatla, D. C. Morton, R. S. DeFries, Y. Jin, and T. T. van Leeuwen (2010), Global fire emissions and the contribution of deforestation, savanna, forest, agricultural, and peat fires (1997–2009), *Atmos. Chem. Phys.*, *10*, 11707–11735, doi: 10.5194/acp-10-11707-2010.

Wang, Y., A. W. DeSilva, G. C. Goldenbaum, and R. R. Dickerson (1998), Nitric oxide production by simulated lightning: Dependence on current, energy, and pressure, *J. Geophys. Res.*, *103*(D15), 19149-19159, doi:10.1029/98JD01356.

Wang, L., M. J. Newchurch, A. Pour-Biazar, S. Kuang, M. Khan, X. Liu, W. Koshak, and K. Chance (2013), Estimating the influence of lightning on upper tropospheric ozone using NLDN lightning data and CMAQ model, *Atmos. Env.*, *67*, 219-228, doi:10.1016/j.atmosenv.2012.11.001.

Williams, E., and S. Stanfill (2002), The physical origin of the land-ocean contrast in lightning activity, *C. R. Phys.*, *3*(10), 1277-1292, doi:10.1016/S1631-0705(02)01407-X.

Yoshida, S., T. Morimoto, T. Ushio, and Z. Kawasaki (2009), A fifth-power relationship for lightning activity from Tropical Rainfall Measuring Mission satellite observations, *J. Geophys. Res.*, *114*, D09104, doi:10.1029/2008JD010370.

Yuan, T., L. A. Remer, K. E. Pickering, and H. Yu (2011), Observational evidence of aerosol enhancement of lightning activity and convective invigoration, *Geophys. Res. Lett*., *38*, L04701, doi:10.1029/2010GL046052.

Zhang, R., X. Tie, and D. W. Bond (2003), Impacts of anthropogenic and natural NO_x sources over the U.S. on tropospheric chemistry, *PNAS*, *100*(4), 1505-1509, doi:10.1073/pnas.252763799.

Ziemke, J. R., S. Chandra, B. N. Duncan, L. Froidevaux, P. K. Bhartia, P. F. Levelt, and J. W. Waters (2006), Tropospheric ozone determined from Aura OMI and MLS: Evaluation of measurements and comparison with the Global Modeling Initiative's Chemical Transport Model, *J. Geophys. Res.*, *111*, D19303, doi:10.1029/2006JD007089.

Table 1. GEOS-5 CCM Biases in Tropospheric Column NO_2[a]

CCM Simulation	RMSE	RMSC	RMSB
noLNOx	0.37	0.26	-0.27
.5xLNOx	0.32	0.24	-0.21
stdLNOx	0.27	0.23	-0.14
2xLNOx	0.24	0.24	-0.02

[a]Calculated with respect to OMIstd column NO_2 for the region bounded by 22°N to 22°S and 180°W to 180°E. RMSE, root-mean-square error; RMSC, centered root-mean-square error; RMSB, root-mean-square bias; all values shown in units of peta molecules cm^{-2}.

Table 2. Mean Tropospheric Column Ozone, CCM, SHADOZ and TES[a]

	Pago Pago, Am. Samoa	Ascension Island	San Cristobal, Galapagos	La Réunion Island
.5xLNOx	24.8	32.3	25.9	45.3
stdLNOx	27.3	37.9	30.1	49.3
2xLNOx	32.3	46.5	36.7	55.5
SHADOZ	25.1	43.6	29.6	49.9
TES_{SHADOZ}	21.4	45.0	31.8	49.4
TES_{ALL}	28.4	46.8	26.3	45.2

[a]Calculated using the dates for which SHADOZ ozonesonde data are available (see Figure 11 caption). Values expressed in Dobson Units.

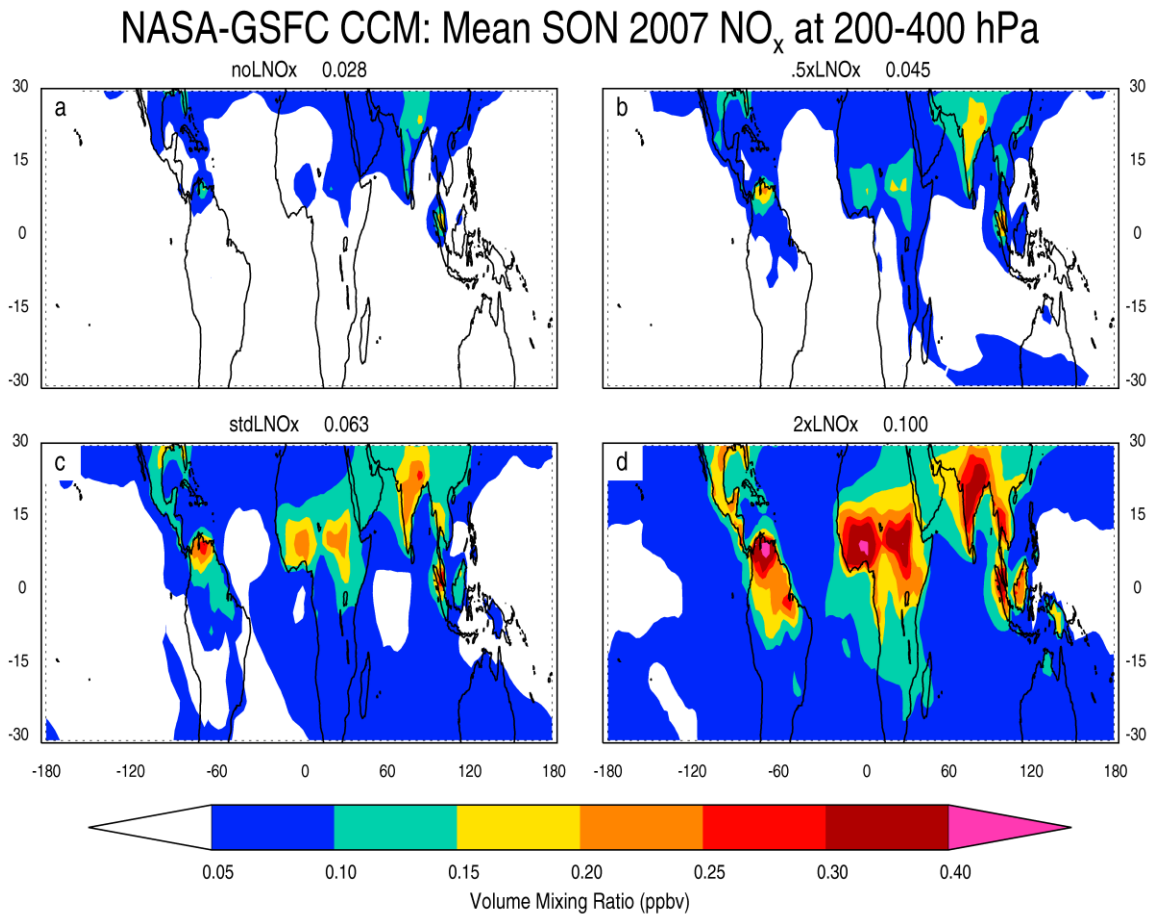

Figure 1. Mean 200- to 400-hPa NO_x, averaged over SON 2007, from the (a) noLNOx, (b) .5xLNOx, (c) stdLNOx and (d) 2xLNOx sensitivity simulations. Regions of greatest change can be seen over northern South America, central Africa and South/Southeast Asia. The value above each panel represents the mean NO_x mixing ratio in ppbv, bounded by 22°N to 22°S.

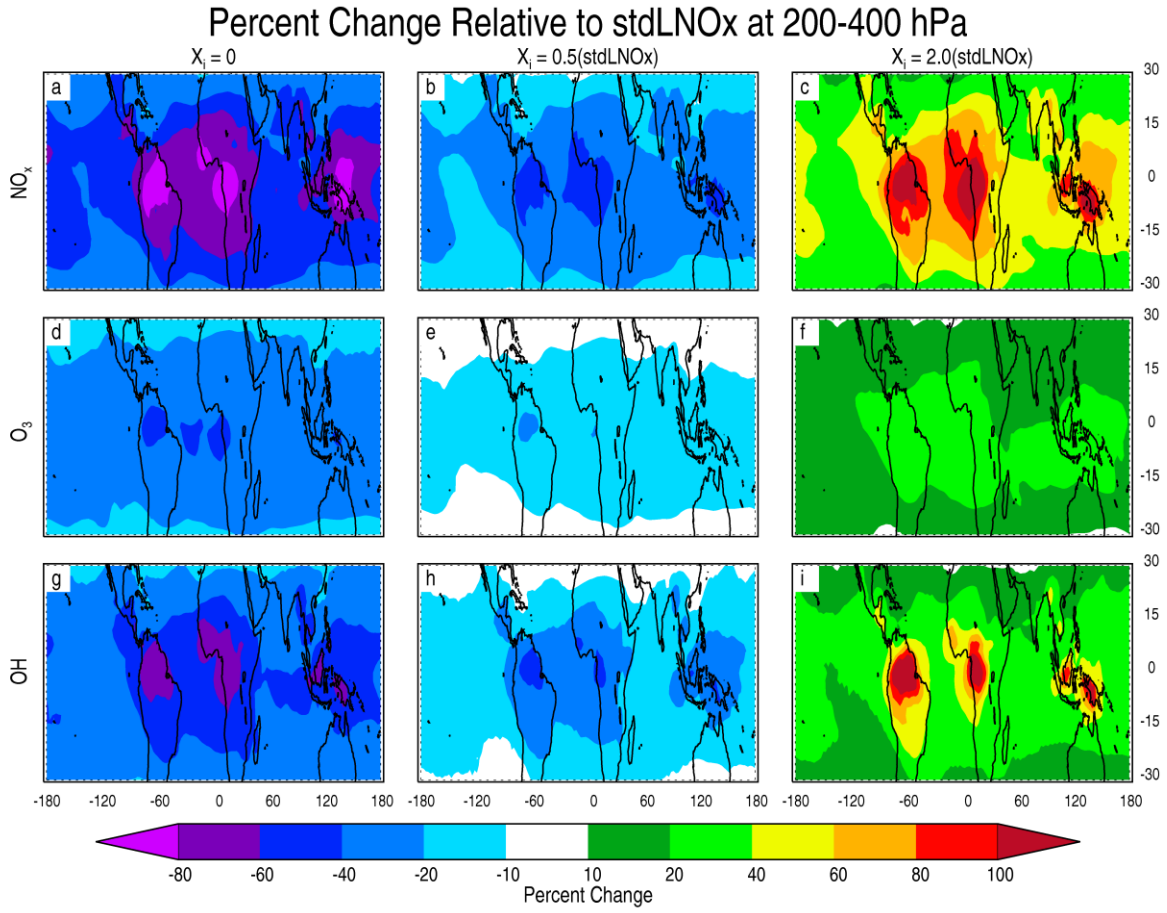

Figure 2. Spatially-distributed percent change in mean 200- to 400-hPa NO_x (a-c), O_3 (d-f) and OH (g-i), relative to stdLNOx. The data represent the SON 2007 average. Percent change is calculated as $[(X_i - \text{stdLNOx}) / \text{stdLNOx}] \times 100$ %, where X_i represents noLNOx, .5xLNOx and 2xLNOx simulations in the left, middle and right columns, respectively.

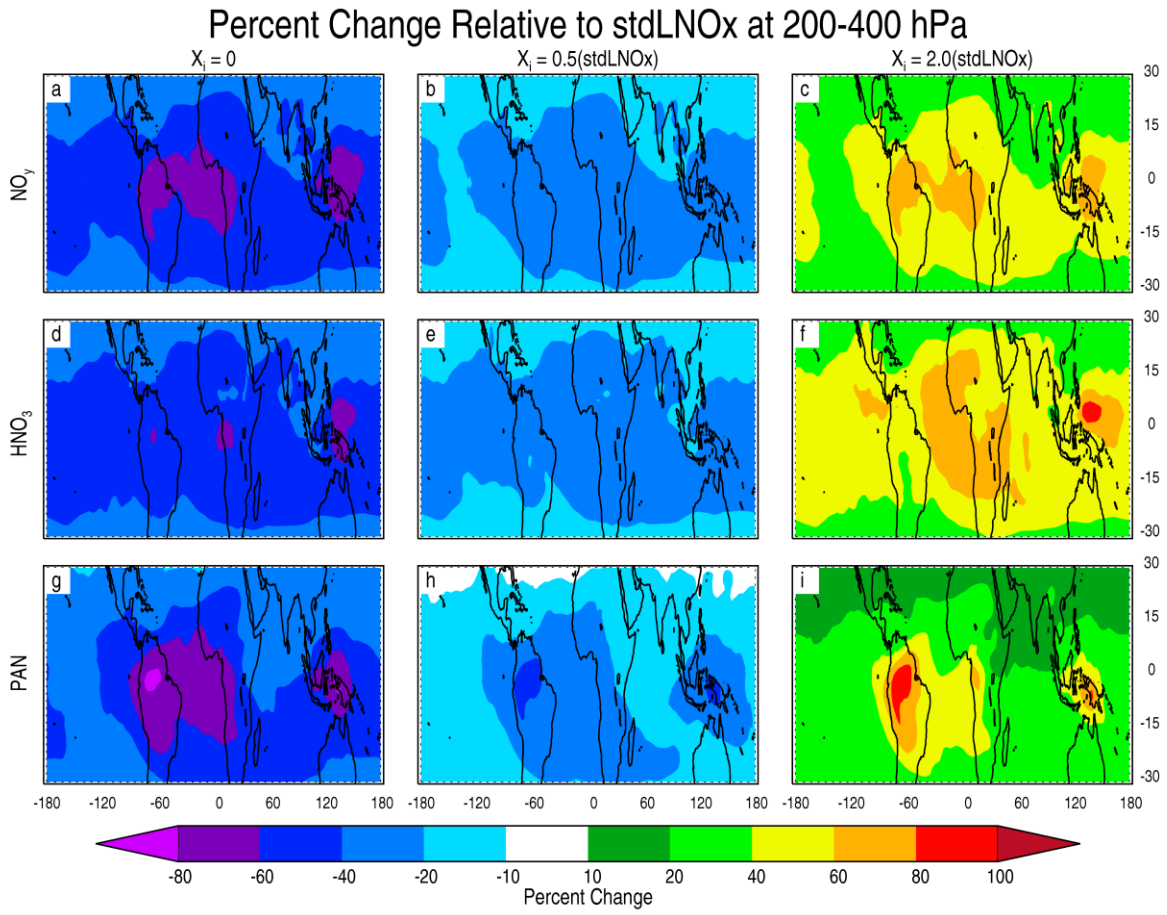

Figure 3. Spatially-distributed percent change in mean 200- to 400-hPa NO_y (a-c), HNO_3 (d-f) and PAN (g-i), relative to stdLNOx. The data represent the SON 2007 average. Percent change is calculated as $[(X_i - \text{stdLNOx}) / \text{stdLNOx}] \times 100$ %, where X_i represents the noLNOx, .5xLNOx and 2xLNOx simulations in the left, middle and right columns, respectively.

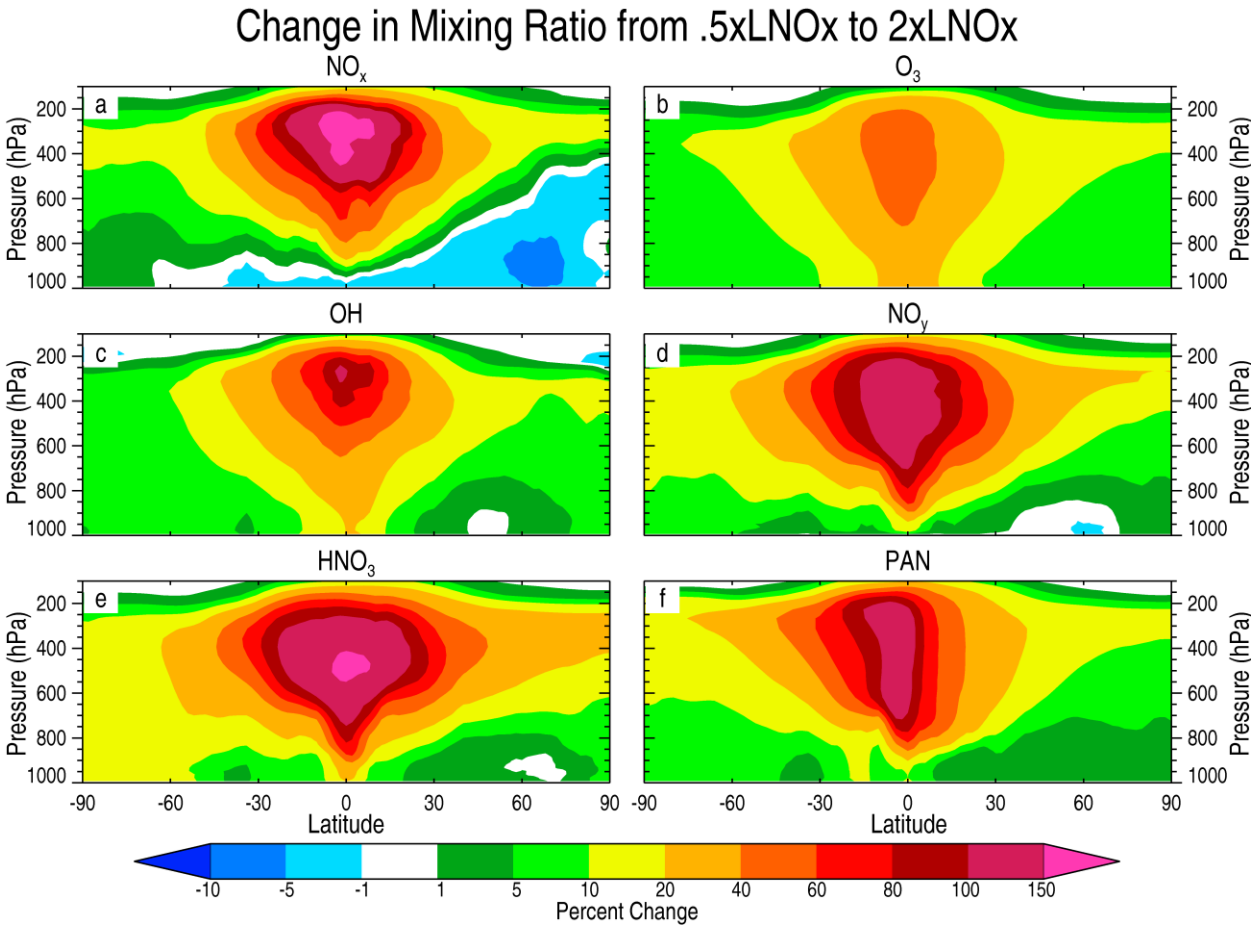

Figure 4. Zonally-averaged percent change in (a) NO_x, (b) O_3, (c) OH, (d) NO_y, (e) HNO_3 and (f) PAN, averaged over SON 2007 and plotted as a function of pressure. Percent change is calculated from .5xLNOx to 2xLNOx as follows: [(2xLNOx – .5xLNOx) / .5xLNOx] × 100 %.

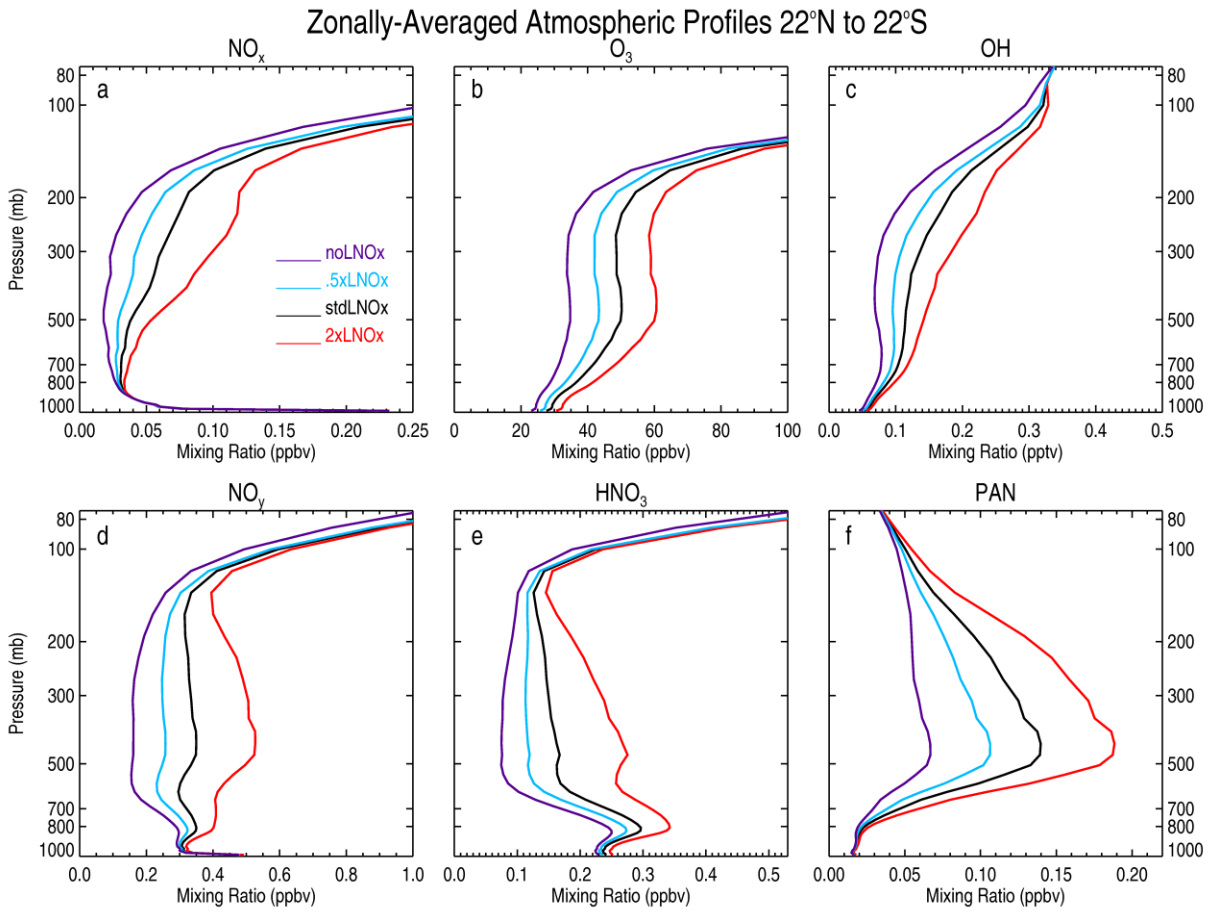

Figure 5. Mean SON 2007 zonal profiles of (a) NOx, (b) O_3, (c) OH, (d) NOy, (e) HNO_3 and (f) PAN, averaged between 22°N and 22°S. The noLNOx (purple), .5xLNOx (cyan), stdLNOx (black) and 2xLNOx (red) mixing ratios are plotted as a function of pressure. Note the difference in the magnitude and the units of the x-axes.

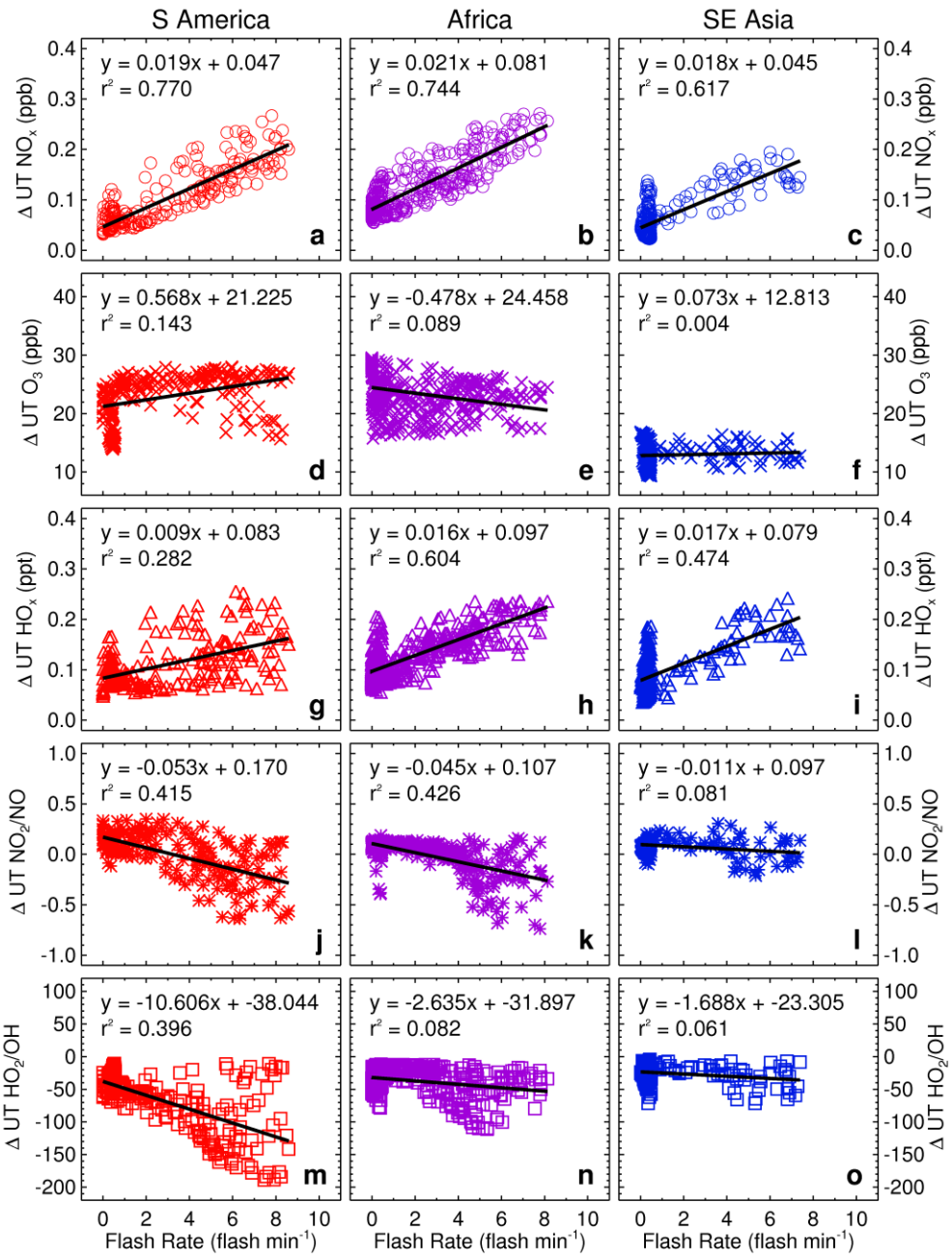

Figure 6. Changes in tropical upper-tropospheric (200 to 400 hPa) NO_x (a-c), O_3 (d-f), HO_x (g-i), NO_2/NO (j-l) and HO_2/OH (m-o) from .5xLNOx to 2xLNOx, versus flash rate, for the SON 2007 time period. Each set of colored symbols represents individual grid points within the titled domain: South America (Red; 22°N to 22°S, 120°W to 40°W), Africa (Purple; 22°N to 22°S, 30°W to 60°E) and Southeast Asia (Blue; 22°N to 22°S, 60°E to 170°E).

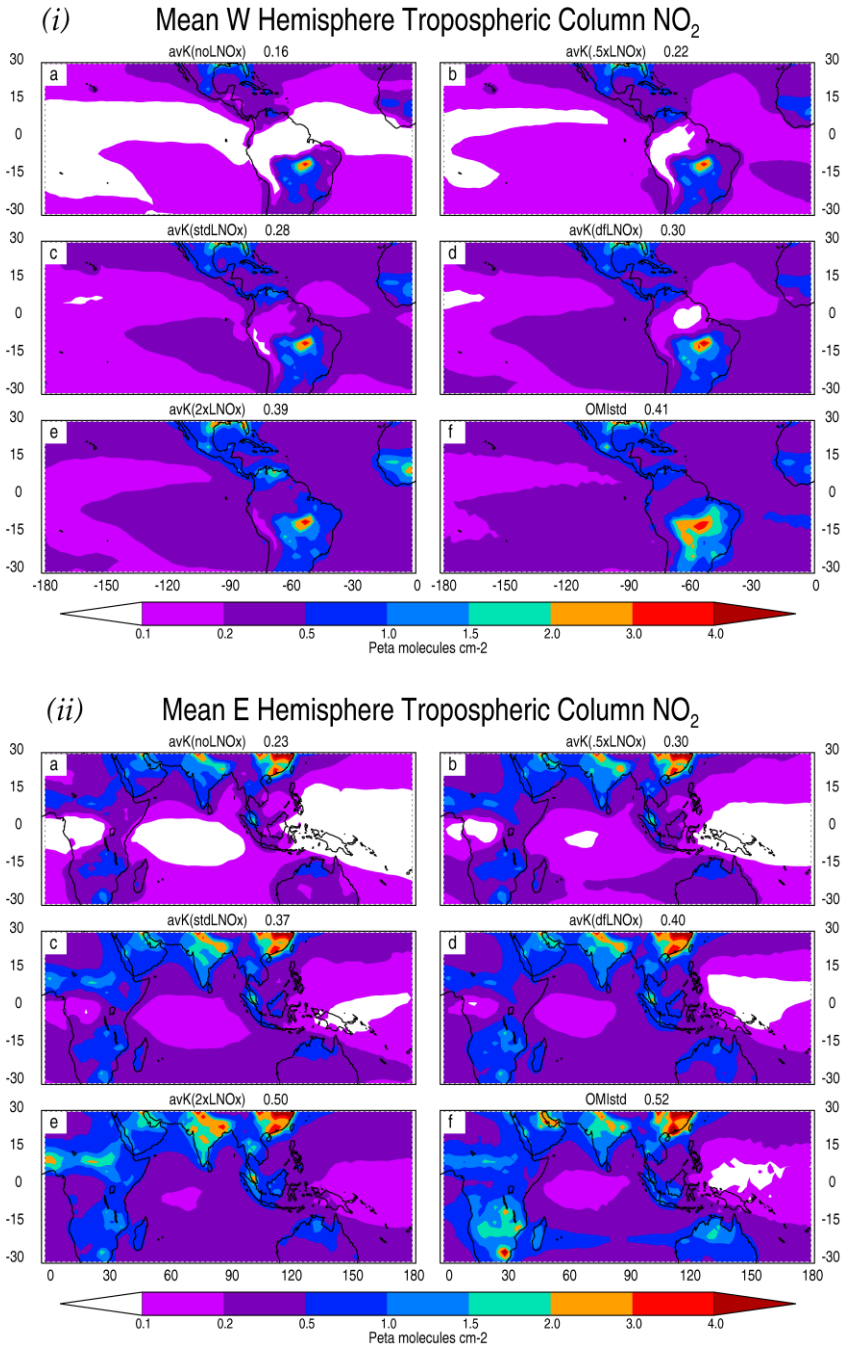

Figure 7. Mean SON 2007 tropospheric column NO_2 for the (i) western and (ii) eastern hemispheres, as simulated by the GEOS-5 CCM (a-e) and as provided by the OMI standard level-2 NO_2 product (f). Panels a through e represent model data after applying the averaging kernel (avK) information included with the OMIstd data. The value above each panel represents the spatially-averaged tropical (22°N to 22°S) NO_2 column in units of peta molecules cm^{-2}.

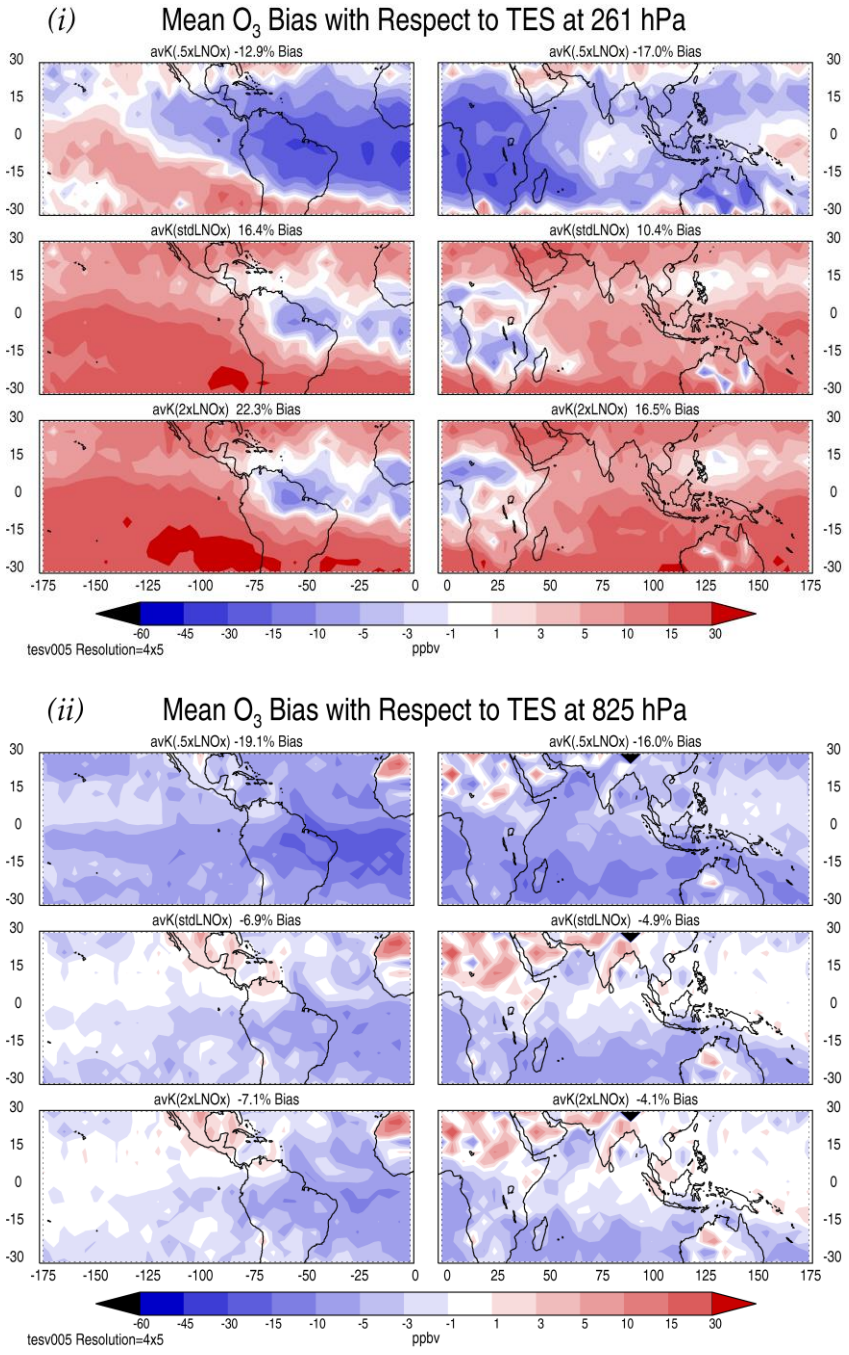

Figure 8. Mean SON 2007 model O_3 biases with respect to the TES version-5 O_3 product for the (i) upper and (ii) lower troposphere. Western Hemisphere (left column) and Eastern Hemisphere (right column) biases are calculated after re-gridding model output to the TES 4° × 5° horizontal resolution and applying the TES averaging kernel information. The percentage listed above each panel represents the mean bias calculated for the tropics (22°N to 22°S).

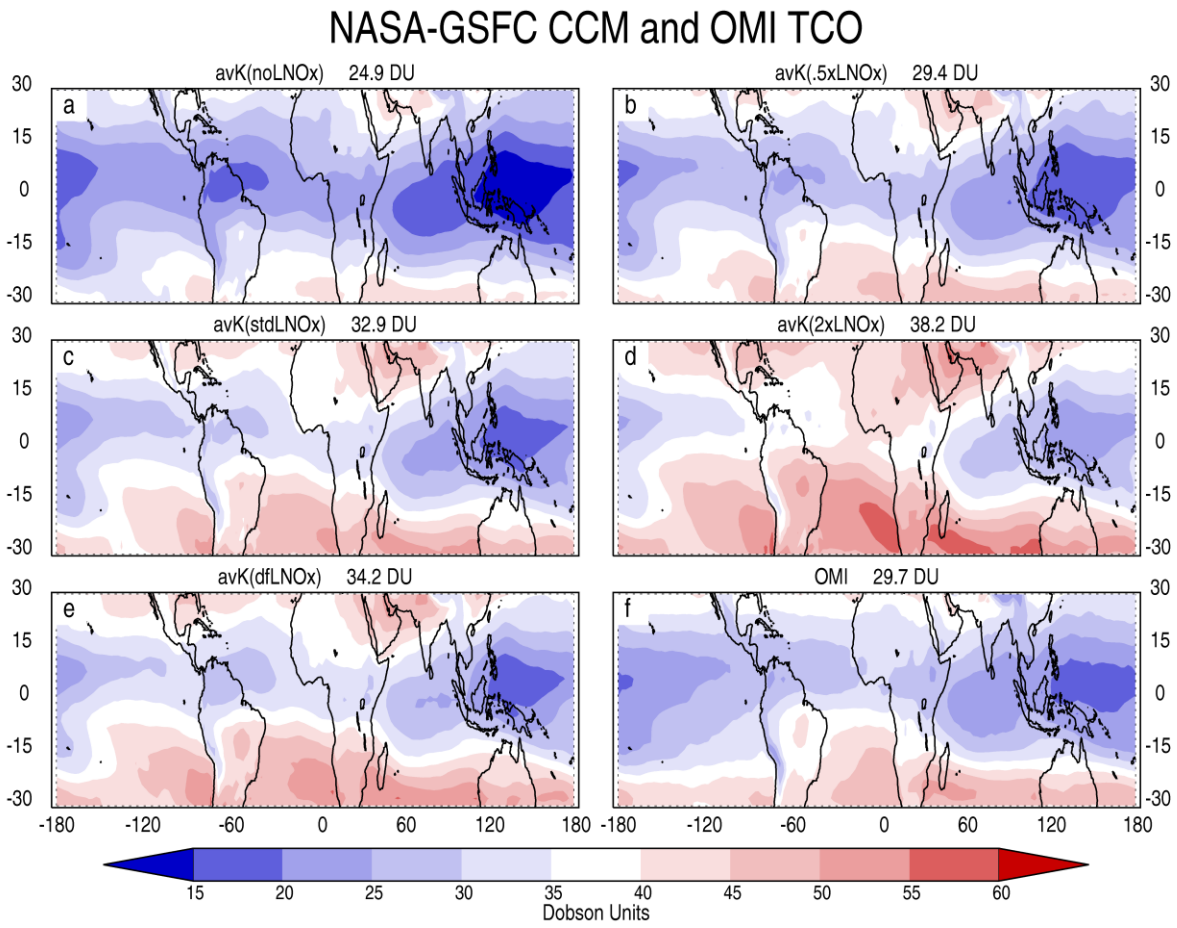

Figure 9. Mean SON 2007 tropospheric column ozone (TCO), as simulated by the GEOS-5 CCM (a-e), and as provided by the level-2 OMI satellite data (f). Panels a through e represent model data after applying the averaging kernel information included with the OMI data product. The value above each panel represents the mean tropical (22°N to 22°S) TCO in Dobson Units.

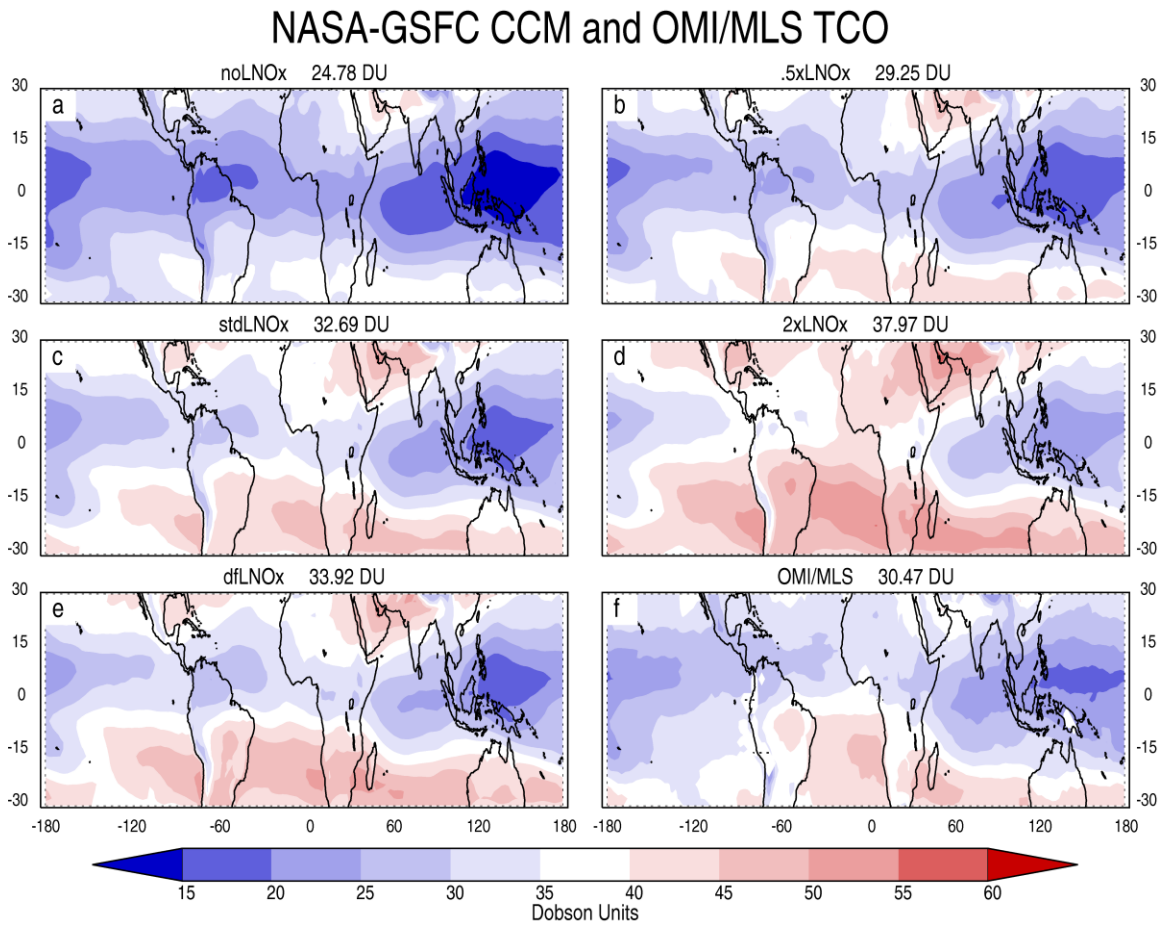

Figure 10. Mean SON 2007 tropospheric column ozone (TCO), as simulated by the GEOS-5 CCM (a-e) and provided by the OMI/MLS TCO data product. The value above each panel represents the mean tropical (22°N to 22°S) TCO in Dobson Units.

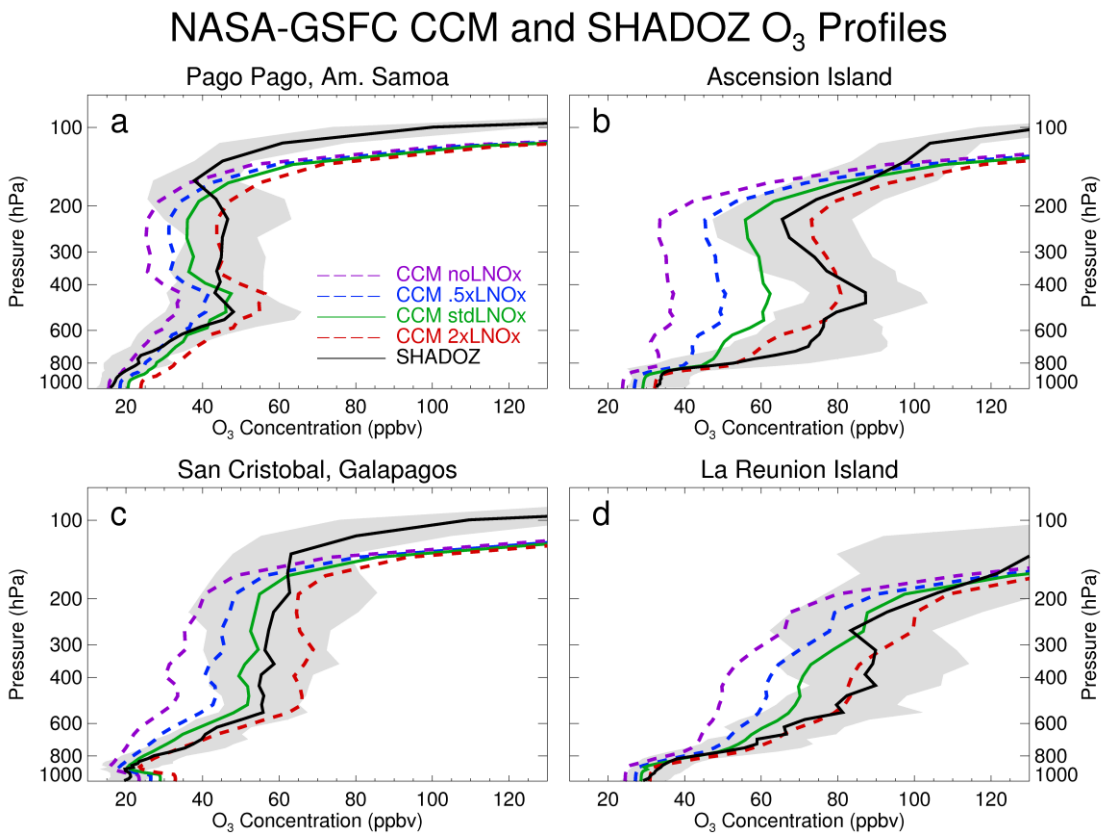

Figure 11. Modeled and observed O_3 profiles over (a) Pago Pago, American Samoa, (b) Ascension Island, (c) San Cristobal, Galapagos and (d) La Réunion Island. Black lines and gray shading represent the mean SHADOZ profile (after re-gridding to the CCM native pressure grid) and the 1-sigma standard deviation (associated with the day-to-day variability), respectively. Colored lines represent CCM profiles, extracted from the model grid box nearest to each SHADOZ location and at the model output time closest to the ozonesonde launch time. Only the dates for which SHADOZ data are available are used in calculating the mean profiles. These available dates are: (a) 21 Sep, 28 Sep, 8 Oct, 15 Oct, 19 Oct, 26 Oct, 2 Nov, 9 Nov, 16 Nov and 25 Nov; (b) 7 Sep, 11 Sept, 25 Sep, 4 Oct, 11 Oct, 18 Oct, 25 Oct, 29 Oct, 5 Nov, 12 Nov, 21 Nov and 28 Nov; (c) 6 Sep, 13 Sep, 20 Sep, 27 Sep, 4 Oct, 11 Oct, 18 Oct, 25 Oct, 1 Nov, 8 Nov, 15 Nov, 21 Nov and 29 Nov; (d) 5 Sep, 12 Sep, 26 Sep, 3 Oct, 17 Oct, 24 Oct, 31 Oct, 7 Nov, 14 Nov, 21 Nov and 28 Nov.

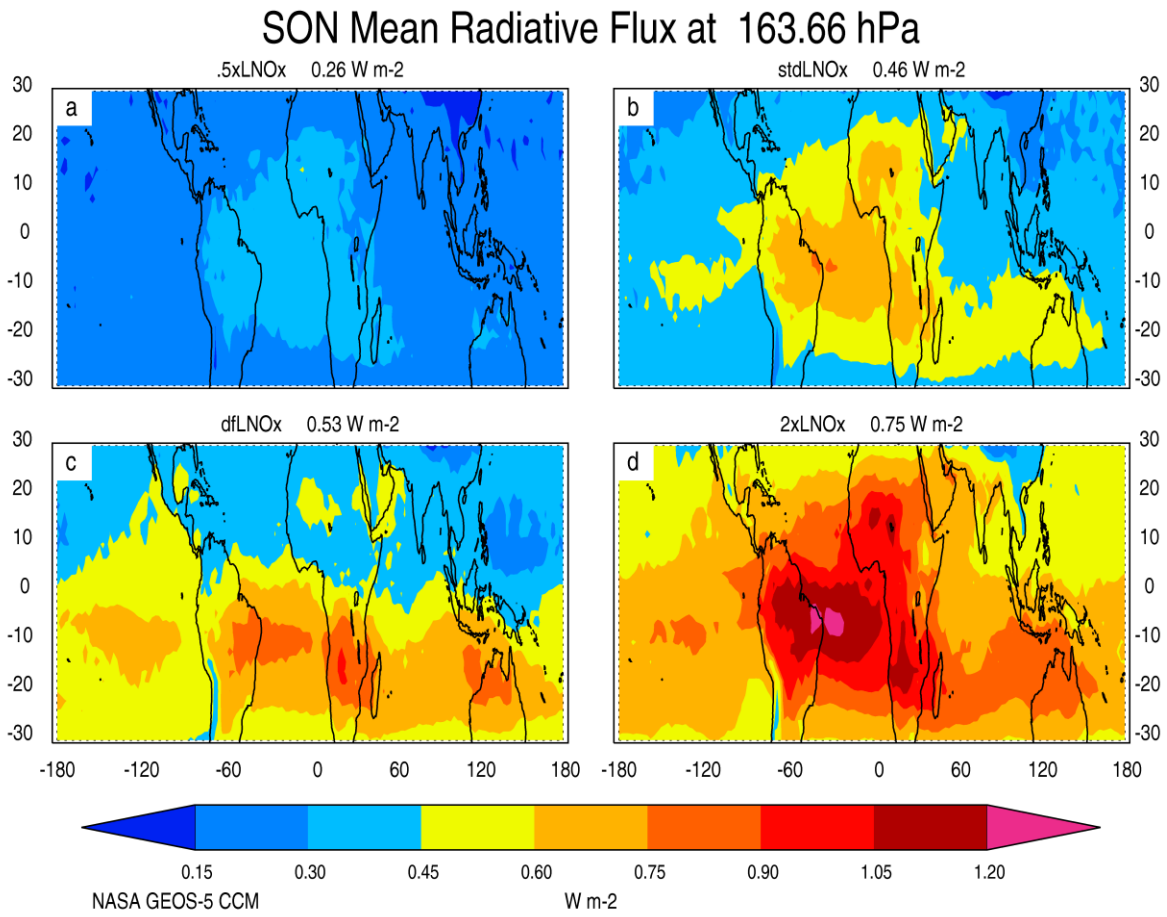

Figure 12. Mean net radiative flux at 163.66 hPa calculated for the (a) .5xLNOx, (b) stdLNOx, (c) dfLNOx and (d) 2xLNOx simulations. Cooler (warmer) colors represent lower (higher) positive flux values in watts per square meter. Values listed above each panel represent the total flux calculated within the 22°N to 22°S domain.

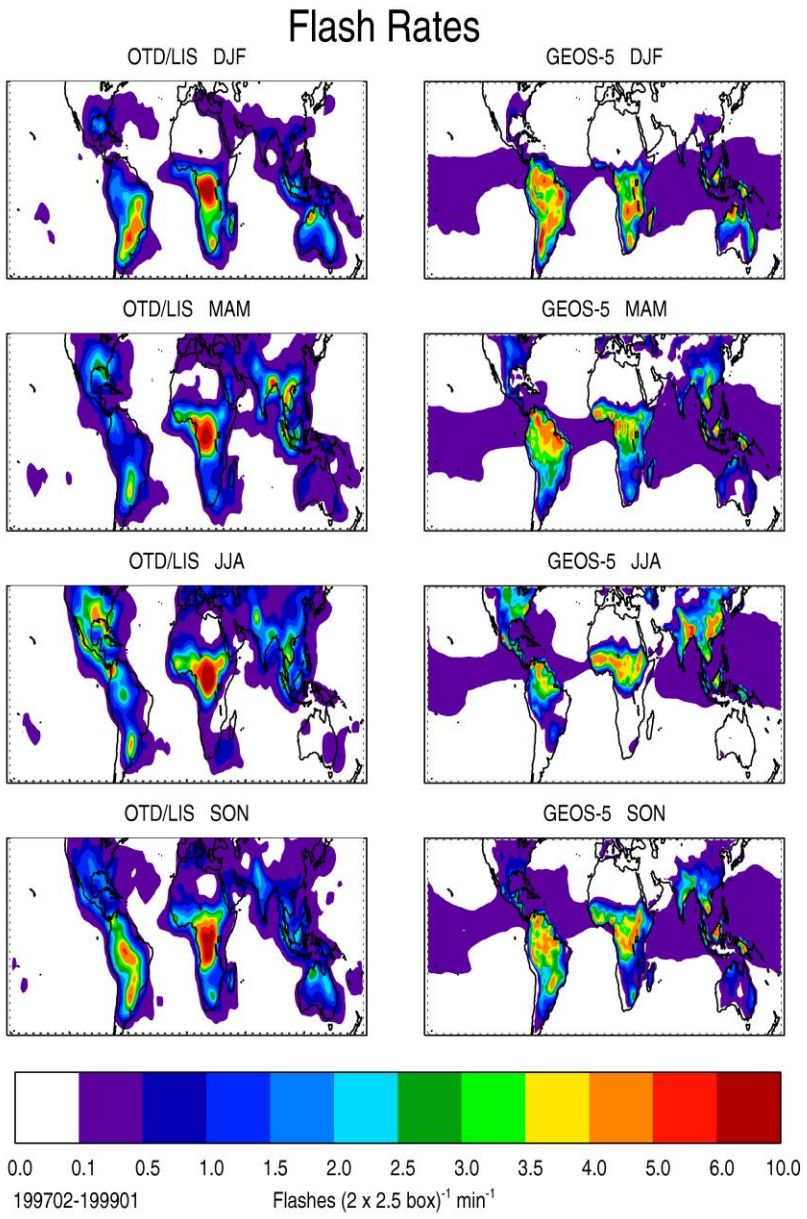

Figure A1. Seasonal model flash rates from the GEOS-5 CCM compared to observed flash rates from OTD/LIS.

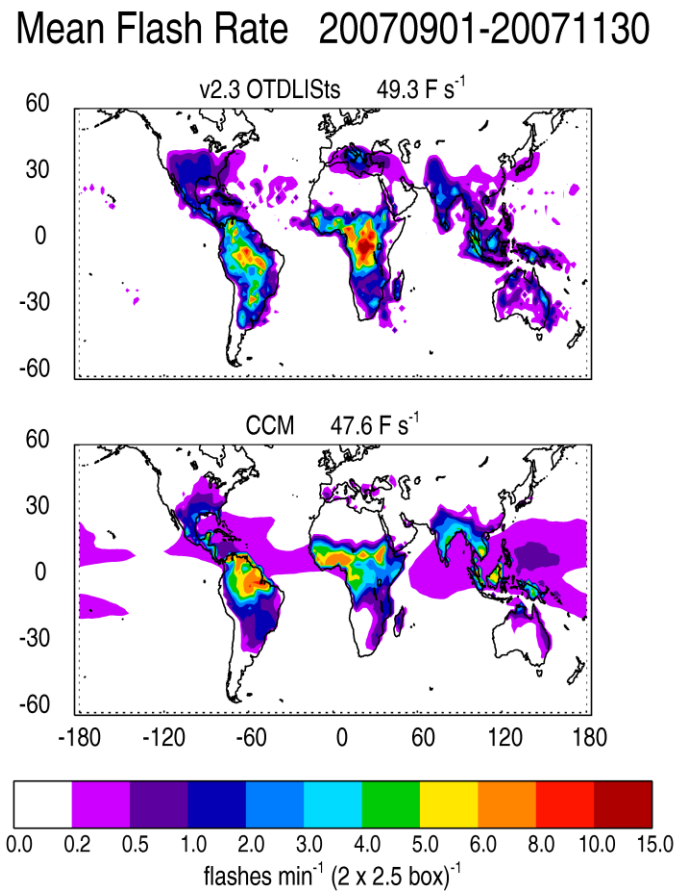

Figure A2. Mean flash rate from OTD/LIS climatology (top) and the GEOS-5 CCM (bottom), expressed as flashes per minute per 2° by 2.5° grid box. Numbers above each panel represent the calculated total flash rate.